



# 1 Combined water table and temperature dynamics control CO<sub>2</sub> 2 emission estimates from drained peatlands under rewetting and 3 climate change scenarios

4 Tanja Denager<sup>1</sup>, Jesper Riis Christiansen<sup>2</sup>, Raphael Johannes Maria Schneider<sup>1</sup>, Peter Langen<sup>3</sup>,  
5 Thea Quistgaard<sup>3</sup>, Simon Stisen<sup>1</sup>

6 <sup>1</sup> Department of Hydrology, Geological Survey of Denmark and Greenland, Copenhagen, Denmark

7 <sup>2</sup> Forest and Landscape Ecology, Department of Geoscience and Nature Management, Copenhagen University,  
8 Denmark

9 <sup>3</sup> Department of Environmental Science, Atmospheric Emissions & Modelling, Aarhus University, Roskilde,  
10 Denmark

11 *Correspondence to:* Tanja Denager (tad@geus.dk)

12

## 13 **Abstract:**

14 This study integrates process-based hydrological modeling and empirical CO<sub>2</sub> flux modeling at a daily  
15 temporal resolution to evaluate how peatland hydrology influence CO<sub>2</sub> emissions under scenarios of  
16 rewetting and climate change.

17 Following the calibration of a three-dimensional transient groundwater flow model for a peat-  
18 dominated catchment, daily groundwater table dynamics were simulated to represent hydrological  
19 conditions in drained peat soils. These simulations were coupled with an empirical CO<sub>2</sub> flux model,  
20 developed from a comprehensive daily dataset of groundwater table depth, temperature, and soil CO<sub>2</sub>  
21 flux measurements. The empirical CO<sub>2</sub> flux model captures a clear temperature-dependent response of  
22 soil CO<sub>2</sub> emissions to variations in groundwater table depth.

23 By applying this coupled modeling framework, we quantified CO<sub>2</sub> emissions at daily timescales. The  
24 results demonstrate that incorporating both temperature sensitivity and high-resolution temporal  
25 variability in water level significantly influences projections of CO<sub>2</sub> fluxes. Especially the co-occurrence  
26 of elevated air temperature and low groundwater table significantly influence CO<sub>2</sub> emissions under  
27 scenarios of rewetting and climate change. These insights highlight the importance of including  
28 changing climate conditions in future peatland management strategies for emission inventories.

29 The study illustrates the value of combining detailed hydrological simulations with emission models. It  
30 also emphasizes the need for detailed monitoring of greenhouse gas emissions across multiple sites  
31 and the development of robust empirical models that can be generalized and spatially upscaled.

32



## 33 Introduction

34 Drained peatlands are widely accepted as being net greenhouse gas (GHG) sources and rewetting of  
35 peatlands is considered an effective means of overall net GHG emission reduction (Leifeld et al., 2019).  
36 The depth of the groundwater table below the surface i.e. the water table depth (WTD) largely  
37 controls the annual emissions of carbon dioxide (CO<sub>2</sub>) and methane (CH<sub>4</sub>) from organic soils, where  
38 deeper WTD results in CO<sub>2</sub> emissions and a shallow WTD increases CH<sub>4</sub> emissions (Evans et al., 2021).  
39 Despite triggering CH<sub>4</sub> emissions, rewetting of organic soils will still lead to a net long-term reduction  
40 of GHG emissions (Günther et al., 2020). However, current estimates of GHG emissions from drained  
41 and rewetted peatlands are still quite uncertain due to a lack of long-term monitoring and simplified  
42 modeling approaches.

43 Commonly adopted methodologies for estimating contribution of organic soils in national GHG  
44 inventories (Arents et al., 2018; Evans et al., 2021; Koch et al., 2023; Tiemeyer et al., 2020) are based  
45 on empirical response functions between long-term annual mean WTD estimates from data-driven  
46 machine learning (ML) models (Bechtold et al., 2014; Koch et al., 2023) and observed net ecosystem  
47 GHG budgets (Tiemeyer et al. 2020). Those methodologies allow regional upscaling and integration  
48 into national emission estimates.

49 However, significant variability in the observed net ecosystem carbon balance (NECB) used to derive  
50 the empirical relationship can be attributed to site-specific factors, including intra-annual (seasonal)  
51 WTD and temperature dynamics (Tiemeyer et al., 2020) caused by fluctuating climate. The current  
52 GHG inventory methods are not suited to account for extremes such as drought and flooding that have  
53 a profound, but temporally limited (days, weeks or months) impact on WTD. Especially the frequency  
54 and severity of droughts can have major impacts on the CO<sub>2</sub> emissions as WTD increases together with  
55 temperature (Olefeldt et al., 2017). Therefore, temperature changes also directly impact GHG  
56 emissions, as soil CO<sub>2</sub> and CH<sub>4</sub> production are temperature sensitive. Currently, the impact of short-  
57 term compound events (e.g., simultaneous warm and dry conditions (Zscheischler et al., 2020) on  
58 annual CO<sub>2</sub> emissions from peat soil is little known. Such events can lead to consequences like a deep  
59 groundwater table, highlighting the need for improved understanding of how climate variability and  
60 long-term change (Olefeldt et al., 2017) affect future CO<sub>2</sub> emissions from both drained and rewetted  
61 peatlands.

62 For Denmark, it is generally expected that, as a result of climatic changes, annual mean WTD will  
63 decrease (water tables closer to terrain). However, this decrease in annual mean WTD is primarily  
64 attributed to an increase in groundwater levels during the wetter winter months, while warmer future  
65 summers are anticipated to experience minimal increase or even reduced summer groundwater levels  
66 and more prolonged drawdowns (Henriksen et al., 2023; Seidenfaden et al., 2022).

67 The ML and statistical models of annual mean WTD (Bechtold et al., 2014; Koch et al., 2023) utilized in  
68 current national GHG inventories (Gyldenkerne et al., 2025; Koch et al., 2023; Nielsen et al., 2025b;  
69 Tiemeyer et al., 2020) effectively reflect the spatial variability at the national scale, but most current  
70 ML WTD models are temporally invariant and do not account for neither inter-annual (between years)  
71 variability, nor seasonality or intra-annual (seasonal) variability in WTD or temperature. To establish  
72 WTD-CO<sub>2</sub> relations at intra-annual time scales, capable of capturing the impact of short-lived extreme  
73 events such as droughts and inundations, WTD time series at these finer temporal resolutions are  
74 required. For this, process-based transient 3D hydrological models capable of integrating unsaturated-  
75 saturated flow models to predict spatial and temporal variability of WTD are highly useful. Combined  
76 with the WTD-CO<sub>2</sub> relation we claim these model outputs can be used to calculate the CO<sub>2</sub> emissions  
77 on daily, seasonal, and inter-annual timescales.



78 Such hydrological models provide the potential for improving our estimation of peatland hydrology  
79 and thereby the spatio-temporal WTD variability. Improved representation of temporal variability of  
80 WTD are needed for refining the current and future GHG estimates that cannot be derived using the  
81 simple application of IPCC default emission factors (IPCC, 2014). Process-based hydrological models  
82 offer the opportunity to assess the effect of different management strategies and environmental  
83 conditions, such as rewetting and climate change.

84 Process-based hydrological models are increasingly being applied to study dynamics of peatland  
85 hydrology (Mozafari et al., 2023). For example through Land Surface Models (LSM) (Bechtold et al.,  
86 2019; Largeron et al., 2018; Shi et al., 2015; Yuan et al., 2021) utilized to analyze the soil–plant–  
87 atmosphere exchange processes of water, energy and carbon. However, most LSM’s rely on a  
88 simplified conceptual representation of hydrologic processes and are characterized by coarse spatial  
89 scales.

90 Of the studies applying fully integrated unsaturated-saturated flow models for peatland hydrology,  
91 some focus on site or field scale models (Friedrich et al., 2023; Haahti et al., 2015; Java et al., 2021;  
92 Stenberg et al., 2018) while others apply the models at catchment scale (Ala-aho et al., 2017; Duranel  
93 et al., 2021; Friedrich et al., 2023; Jutebring et al., 2018; Lewis et al., 2013). A catchment scale  
94 approach with water balance closure is particularly important for climate change impact predictions,  
95 since the boundary conditions to the peatlands will also be affected by climate change. Similarly, the  
96 use of catchment scale models is important because impact evaluations of peatland management  
97 scenarios, such as rewetting, can also include impacts on streamflow and groundwater levels in  
98 neighboring areas.

99 The objectives of this study were to 1) estimate current and predict the future hydrology and soil CO<sub>2</sub>  
100 emissions in a Northern European drained peatland and 2) investigate the role of rewetting and  
101 climatic extremes on annual CO<sub>2</sub> emissions. To achieve these objectives, we used a transient  
102 physically-based hydrological 3D model to predict daily WTD for a case study area, the Tuse Stream  
103 catchment, representing a typical degraded Danish peatland. Secondly, we developed an empirical soil  
104 CO<sub>2</sub> flux (fCO<sub>2</sub>) model based on coupled CO<sub>2</sub> flux, WTD and temperature observations for a similar  
105 Danish peatland (Nielsen et al., 2025a), capable of making daily predictions. Combining the  
106 mechanistic hydrological model and the empirical emission model enabled the estimation of daily soil  
107 CO<sub>2</sub> fluxes under current conditions as well as scenarios of rewetting and future climate, while  
108 accounting for the impact of climatic variability and extremes.

## 109 Data and methodology

### 110 Study area

111 Tuse Stream catchment is located on the island of Zealand in the eastern part of Denmark (Figure 1a).  
112 The total area encompasses 107 km<sup>2</sup> of which 19 km<sup>2</sup> are peat soil. The areal extent of peat soil was  
113 determined using a national map of organic soils (Adhikari et al., 2014). The largest contiguous peat  
114 area within the catchment is a 13 km<sup>2</sup> drained fen located in a river valley (Figure 1c) in the low-lying  
115 part of the catchment. The peat soil area is primarily used for agriculture. In small parts of the area,  
116 the drainage has been stopped to restore the natural hydrologic regime. The measured peat layer  
117 thickness extends from 0.4 to 3.5 meters, below which alluvial sand deposits are typically found.  
118 Generally, the deeper geology in the area can be characterized as clay-dominated glacial till deposits.  
119 The catchment is characterized by flat topography, with the southern part of the catchment being  
120 hillier. The climate conditions are humid and temperate. The catchment receives about 737 mm of  
121 precipitation per year (1990-2024) and has an annual mean temperature of 9°C (Scharling, 1999a, b).

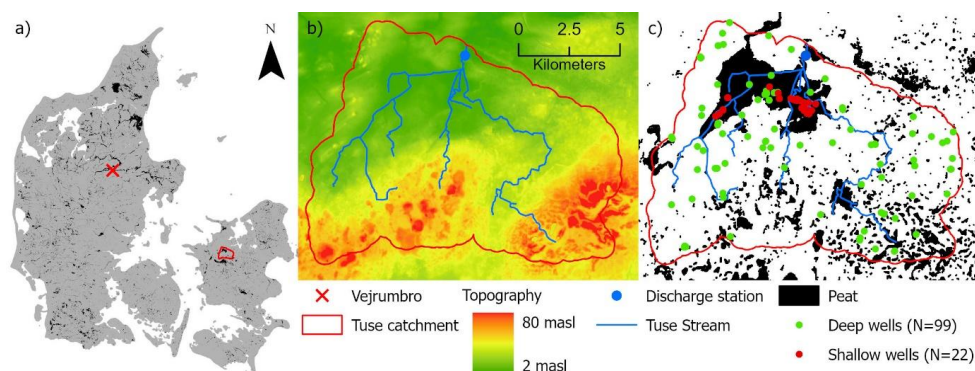


Figure 1: a) Location of Tuse Stream catchment and the Vejrumbro site, b) topography and stream network of Tuse Stream catchment, masl: meter above sea level, c) location of organic soil and observation wells in the Tuse Stream catchment.

Shallow WTD in the drained organic soils is monitored in 22 groundwater wells (2-3.5 meters deep) (Figure 1c). The wells are fully screened and WTD is automatic logged with pressure transducers at an hourly basis (aggregated to daily values) and verified with manual measurements. All WTD data are available in the Danish National Well Database (Jupiter, 2025). In this study, we define the water table depth (WTD) as positive when located below the terrain and negative when above the terrain. Monitoring data includes additional point measurements and timeseries of groundwater head from 99 deep wells installed in mineral soils throughout the catchment (Figure 1c). In the model setup, water extraction in 40 abstraction wells is included based on data from the Danish National Well Database in May 2020 (Henriksen et al., 2020) and implemented as yearly mean abstraction evenly distributed on the daily model timesteps. Daily discharge is monitored at the catchment outlet at Tuse Stream (Figure 1b).

## Hydrological modelling

The focus of the hydrological modelling in this study is to adequately simulate shallow groundwater levels and their dynamics for the peatland area in the Tuse Stream catchment. The fen peatland in Tuse Stream catchment is largely fed by groundwater discharge from the upstream catchment, emphasizing the need to develop a coupled groundwater surface water model at catchment scale. In addition, the objective of utilizing the model for climate change impact assessments requires a catchment scale approach with a deep groundwater component to represent changes in groundwater and surface water discharge to the peatland as well as changes in the boundary conditions. The catchment scale approach also facilitates the combined calibration and evaluation of the total water balance and peatland WTD by constraining the model with observed streamflow at the outlet as well as peatland groundwater level dynamics.

The model is set up as a transient, distributed, coupled surface-groundwater model and executed within the hydrological modeling framework MIKE SHE (DHI, 2022; Graham and Butts, 2005). MIKE SHE combines full 3D groundwater flow coupled with a gravity flow module in the unsaturated zone, 2D overland flow and 1D river flow routing in streams (DHI, 2019) (Figure S1). The simplified gravity flow module for unsaturated flow assumes a uniform vertical gradient and ignores capillary forces but provides a suitable solution for the time varying recharge to the groundwater table based on precipitation and evapotranspiration (DHI, 2022).

The model is a modified sub-model of the National Hydrological Model of Denmark (DK-model), developed at the Geological Survey of Denmark and Greenland (GEUS) (Henriksen et al., 2020; Stisen et al., 2019). The geological model is interpreted in a horizontal 100 meter grid. The numerical model is



157 calibrated in the same 100 meter resolution, with the saturated zone consisting of 11 computational  
158 layers of varying thickness. The top model layer has a uniform thickness of 2 meters, which is also  
159 applied to the peat layer areas. The bottom level of the groundwater model is defined by the  
160 prequaternary chalk that underlies the Island of Zealand, which in the Tuse Stream catchment is  
161 located in a depth of approximately 150-250 meters below surface.

162 The time-varying constant head boundary conditions at the sub-model boundary are defined from the  
163 operational National Hydrological Model setup (Henriksen et al., 2020). The observed forcing data of  
164 precipitation, temperature and reference evapotranspiration are provided by the Danish  
165 Meteorological Institute (DMI) as gridded daily data in 10 km resolution for precipitation and 20 km  
166 resolution for evapotranspiration and temperature (Scharling, 1999a, b; Stisen et al., 2011). The model  
167 employs a maximum timestep of one day, at which the meteorological variables are fed into the  
168 model. The model was provided with a hotstart file from an initial model run.

169 Spatial and temporal distributions of root depth and LAI are based on classes (Figure S2 and Table S1)  
170 where the peat, forest, agricultural and open nature land use classes have yearly cycles of LAI and root  
171 depth (Figure S3). Likewise, soil type is spatially distributed (Figure S2) and based on the three classes  
172 peat, sand and clay (Table S2). In the vertical direction, the soil columns in the unsaturated zone  
173 module are divided into 40 cells from top to bottom; 30x0.1m, 5x1m and 5x5m. Technically, the  
174 unsaturated zone is parameterized to 33 m depth, but during simulation limited to the top of the  
175 simulated groundwater table. We implemented uniform vertical water retention characteristics of  
176 peat, while clay and sand water retention characteristics were defined separately for the depths 0-30  
177 cm (horizon A), 30-70 cm (horizon B) and >70 cm (horizon C). Soil parameterization is freely adapted  
178 from (Børgesen et al., 2009) and detailed in Table S3.

179 MIKE SHE allows incorporation of drainage systems, representing both artificial and natural drains. The  
180 drainage system bypasses the slow water movement in aquifers by providing a short-cut from e.g. the  
181 agricultural field to the nearest stream. The amount of water routed by drains from the saturated zone  
182 to local surface water bodies is calculated using a linear reservoir model, where the difference  
183 between groundwater head and drain level is multiplied by a drain time constant ( $dt$ ). The drain level is  
184 defined by a drain depth ( $dd$ ) set relative to terrain level. Hence, drainage in any given model cell only  
185 occurs if the simulated groundwater level exceeds the drainage level (DHI, 2022). The drain time  
186 constant and drainage depth in each model grid cell are distributed across the model domain  
187 according to the five land use classes (Figure S2 and Table S1).

188 The model parameter sensitivity analysis and subsequent calibration prioritized parameters affecting  
189 the shallow WTD in the peat soil and the overall water balance in the catchment. A list of model  
190 parameters can be seen in Table S3. Parameter values not included in the calibration process are  
191 obtained from the National Hydrological Model parametrization.

## 192 Calibration method

193 We used the Pareto Archived Dynamically Dimensioned Search (PADDs) algorithm (Asadzadeh and  
194 Tolson, 2013) available within the optimization toolkit Ostrich (Matott, 2019). PADDs is a multi-  
195 objective optimizer and obtains the pareto front across multiple objective function groups, enabling  
196 post-weighting of individual objective functions. Throughout the calibration routine, Ostrich minimized  
197 the weighted sum of squared error (WSSE) of the objective functions. The PADDs algorithm was run  
198 with the user settings of maximum 1000 iterations. The period 2010-2013 was used as a calibration  
199 spin-up period and the model performance was evaluated for the 2014-2023 calibration period.

200 Calibration was performed against three objective function groups within the categories of WTD in  
201 shallow groundwater wells located in drained organic soils (modified  $KGE_{WTD}$ ), spatial correlation of the



mean WTD ( $r_{spatial}$ ) and a combined objective function group of discharge, hydraulic head level and seasonal amplitude in deeper wells ( $q\_head\_amp$ ). The multi-objective optimization problem can be formulated as:

$$\min \left( q\_head\_amp, 1 - KGE_{WTD_{modified}}, 1 - r_{spatial} \right) \quad [1]$$

The metrics used as response variable in the objective functions on the three-dimensional pareto front can be seen in Table 1.

Kling-Gupta Efficiency ( $KGE_q$ ) was used as a conventional performance criterion for discharge. The  $KGE$  consists of three terms: the Pearson correlation coefficient  $r$ , a term representing the measure of variability  $\alpha$ , and a bias term  $\beta$ .  $KGE_q$  is included to match the overall water balance and streamflow dynamics expressed through the discharge at the catchment outlet.  $ME_{head}$  was included in the objective function to match the general water level in the deeper aquifers across the catchment, and  $ME_{amp}$  to represent the natural seasonal variations as a mean error of yearly amplitude for hydraulic head for deep wells with continuous time series. For a detailed description of the implementation of  $ME_{amp}$  as objective function see (Henriksen et al., 2020).  $KGE_q$ ,  $ME_{head}$ ,  $ME_{amp}$  were equally weighted (according to WSSE from an initial model run) in the combination of the three metrics into one objective function ( $q\_head\_amp$ ).

$KGE$  was likewise used as performance criterion for WTD, however in a modified version ( $KGE_{WTD_{modified}}$ ). Conventionally,  $\beta$  in  $KGE$  is a unitless measure of the bias specified as the ratio between the sum of simulated and observed values ( $\beta = \sum sim / \sum obs$ ). As we optimize against the WTD, the operational sign can be both negative (water table above terrain/inundation) and positive (water table below terrain), violating the idea of optimizing  $\beta$  as the ratio of sums of values with possibly alternating operational signs. Therefore, we are using a modified  $KGE_{WTD}$  where  $\beta$  is replaced by the mean error (ME), see Table 1. This modification requires that the order of magnitude of the  $ME_{WTD}$  is comparable to the errors on the other terms in  $KGE$ . In our case this is ensured by the fact that the mean observed WTD values range between approximately 0.3-0.6 m, resulting in  $ME_{WTD}$  values typically below 0.5 m. Alternatively, the  $ME_{WTD}$  term could be scaled within the  $KGE_{WTD}$  equation.

The calibration using the modified  $KGE_{WTD}$  aims at achieving the best overall agreement between simulated and observed WTD. Consequently, a perfect match at individual monitoring wells is not anticipated; instead, the goal is to achieve a general fit that represents the optimal compromise across all wells. In order to optimize the spatial variability of the mean WTD, the correlation coefficient ( $r_{spatial}$ ) was included as objective function.





240 Table 1: Objective functions metrics. KGE stands for Kling-Gupta Efficiency.

Objective function	Observations	No. of observation wells	Metric	Abbreviation	Equation	Range	Optimum value
Modified KGE <sub>WTD</sub>	Daily WTD in shallow wells (in peat)	22	Modified KGE on WTD	KGE <sub>WTD,modified</sub>	$1 - \sqrt{(r_{WTD} - 1)^2 + (\alpha_{WTD} - 1)^2 + (ME_{WTD})^2}$ Where, $ME_{WTD} = \frac{1}{n} \sum_{i=1}^n WTD_{sim_i} - WTD_{obs_i}$	$[-\infty; 1]$	1
r <sub>spatial</sub>	Mean WTD over the calibration period	22	Spatial correlation of the mean WTD	r <sub>spatial</sub>	$r(WTD_{sim}, WTD_{obs})$	$[-1; 1]$	1
q <sub>head_amp</sub>	Discharge	1	KGE on discharge	KGE <sub>q</sub>	$1 - \sqrt{(r_q - 1)^2 + (\alpha_q - 1)^2 + (\beta_q - 1)^2}$	$[-\infty; 1]$	1
	Hydraulic head in deep wells (in mineral soil)	66	Mean error on hydraulic heads	ME <sub>head</sub>	$\frac{1}{n} \sum_{i=1}^n head_{sim_i} - head_{obs_i}$	$[-\infty; \infty]$	0
		8	Mean error on yearly amplitude of hydraulic heads	ME <sub>amp</sub>	$\frac{1}{n} \sum_{i=1}^n A_{sim_i} - A_{obs_i}$	$[-\infty; \infty]$	0

241 WTD: water table depth [m], q: discharge [m/s], head: hydraulic head [m], A: amplitude [m]

242 A local sensitivity analysis based on initial parameter values from Table S4 was performed and values  
 243 of composite scaled sensitivity (CSS) were obtained. Selection of free calibration parameters were  
 244 based on the criterion that parameters were included if their CSS was larger than 0.05\*CSS of the  
 245 parameter with the highest CSS. The resulting 11 free parameters are indicated with grey in Table S4.  
 246 Other parameters were kept at the values listed in Table S4 or tied to the calibration parameters.

247 Hydrological simulations of historical and future climate

248 The calibrated hydrological model was run for the historical simulation period of 1990-2023 using  
 249 observed climate forcing data (Scharling, 1999a, b; Stisen et al., 2011). Future hydrological projections  
 250 are derived from simulations using the hydrological model forced by climate model projections,  
 251 including precipitation, air temperature (T<sub>air</sub>), and potential evapotranspiration. The resulting impacts  
 252 on groundwater levels, as simulated by the hydrological model, are evaluated. We used 17 climate  
 253 models (Table S5) with the Representative Concentration Pathway 8.5 (RCP8.5). The climate model  
 254 outputs are generated and bias corrected by Pasten-Zapata et al. (2019), and the Global and Regional  
 255 Circulation (GCM, RCM) models originate from the Euro-CORDEX project (Jacob et al., 2014).

256 The climate simulations cover three 30-year periods: the reference period (1991-2020), the near future  
 257 (2041-2070) and the distant future (2071-2100). All 51 climate simulations (17 climate models × 3  
 258 periods) were first run using the initial potential head from the national model climate simulations  
 259 (Henriksen et al., 2020). Subsequently, they were rerun using the mean potential head for the  
 260 respective 30-year period as the initial potential head.

261 Empirical CO<sub>2</sub> emission models

262 Implementation of annual CO<sub>2</sub> emission model

263 Recent studies established a functional relationship between the annual net ecosystem carbon balance  
 264 (NECB) for CO<sub>2</sub> and the mean annual WTD (Koch et al., 2023; Tiemeyer et al., 2020) by fitting a  
 265 nonlinear Gompertz function. Like in Koch et al. (2023) and Tiemeyer et al. (2020), this study considers



NECB as only CO<sub>2</sub> fluxes, excluding methane (CH<sub>4</sub>) and other carbon exports such as dissolved or particulate organic carbon. We apply the WTD functional relationship for CO<sub>2</sub> from Koch et al. (2023), which is fitted to Danish flux data, and refer to it as the *Annual WTD model*. The *Annual WTD model* demonstrates a systematic relationship in which CO<sub>2</sub> flux from NECB increases with annual WTD in the interval between 7 cm and 50 cm, above which an asymptotic level of 10 Mg CO<sub>2</sub>-C ha<sup>-1</sup> yr<sup>-1</sup> is reached (Koch et al., 2023). The *Annual WTD model* is therefore not sensitive to changes in WTD deeper than approximately 50 cm. At WTD levels less than 7 cm, the *Annual WTD model* suggests CO<sub>2</sub> uptake; however, this element is not included in our analysis which only models CO<sub>2</sub> emission.

Derivation and implementation of daily CO<sub>2</sub> emission model  
For our empirical model to predict daily soil CO<sub>2</sub> fluxes (fCO<sub>2</sub>) we assume that the WTD dependent NECB (Tiemeyer et al. 2020, Koch et al. 2023) is driven mainly by the response of soil respiration to WTD and T<sub>air</sub>, as gross primary photosynthesis (GPP) and aboveground autotrophic respiration is mostly dependent on light availability and plant phenology (Rodriguez et al., 2024). This allows scaling to match the NECB magnitude but maintains integrity in the regulation of WTD on soil CO<sub>2</sub> fluxes.

Using a unique and comprehensive coupled dataset (Nielsen et al., 2025a) of daily mean net soil CO<sub>2</sub> fluxes, T<sub>air</sub> and WTD for six spatial replicate measurement points, we develop a coupled temperature and WTD dependent empirical soil CO<sub>2</sub> flux model, hereafter referred to as the *Daily WTD-T<sub>air</sub> model*. The model essentially scales the WTD-fCO<sub>2</sub> relation to T<sub>air</sub>. The dataset Nielsen et al. (2025a) is from a drained fen, called Vejrumbro (Figure 1), with similar characteristics (soil type, climate, land use history) as the peat area in the Tuse Stream catchment (see methodological details in Nielsen et al. (2025a)). The soil net CO<sub>2</sub> fluxes, WTD and T<sub>air</sub> were measured automatically for one year (2022-2023) (Nielsen et al., 2025a) and we used a subset of fluxes

measured for six spatial replicates 5-6 times per day, resulting in a dataset of 10950 – 13140 individual fluxes covering 365 days (Nielsen et al., 2025a).

Implementation of CO<sub>2</sub> flux models  
Spatially distributed net soil CO<sub>2</sub> fluxes are calculated at a 100-meter scale across the 13 km<sup>2</sup> contiguous peatland area (Figure 1) with the *Annual WTD model* and the *Daily WTD-T<sub>air</sub> model*, respectively, using WTD at a 100-meter scale (hectare scale) and a uniform T<sub>air</sub>. Afterwards the spatially distributed soil CO<sub>2</sub> fluxes are aggregated to represent the spatial mean of the 13 km<sup>2</sup> peatland area.

First, we applied the *Annual WTD model* and the *Daily WTD-T<sub>air</sub> model* for the historical simulation period of 1990-2023, using spatiotemporal distributed WTD from the calibrated hydrological model. Afterwards, the empirical CO<sub>2</sub> models are utilized on each of the 17 climate projections for T<sub>air</sub> and WTD. Daily T<sub>air</sub> for the Tuse Stream catchment peatland area is taken directly from the 17 bias corrected climate projections, while daily spatial WTD is a model output from the 17 hydrological simulations, when running the hydrological model with the forcing data (precipitation, temperature and evapotranspiration) from the 17 climate projections. Thereby, we are able to quantify the variability in soil CO<sub>2</sub> flux among the 17 climate projections for each of the simulation periods and among the 30 years within each of the simulation periods.

Design and application of rewetting scenarios  
For impact evaluations of peatland management scenarios, such as rewetting, on the annual CO<sub>2</sub> emissions, we define three rewetting scenarios: A, B and C. These scenarios are implemented through controlled modifications of the simulated WTD in peatland grid cells. This method of representing rewetting scenarios does not involve structural modifications to the hydrological model and assumes changes in WTD without accounting for process-based feedback mechanisms within the coupled





311 surface–subsurface hydrological system. All rewetting scenarios are applied for the entire historical  
312 period from 1990 to 2023 and thereby representing the climatology conditions for this period and  
313 producing three 34-year time series of rewetted WTD.

314 The scenarios are meant to illustrate different rewetting impacts on WTD, representing wetter winters  
315 (A), uniform shift in WTD (B) and wetter summers (C), but all with the same long-term mean WTD. In  
316 Scenario A, the daily groundwater table is elevated when it is above the long-term (34-year) mean  
317 water table resulting in unchanged water table levels during summer but an increase in winter.  
318 Scenario B uniformly raises the water table by a constant scalar, while Scenario C applies the same  
319 scalar increase to water table while simultaneously reducing the annual amplitude by half. The  
320 modifications of the simulated WTD are implemented using the following equations:

$$321 \quad WTD_{i_{rewet A}} = \begin{cases} WTD_i, & \text{if } WTD_i \geq \overline{WTD} \\ WTD_i + 2.5 \cdot (\overline{WTD} - WTD_i), & \text{if } WTD_i < \overline{WTD} \end{cases} \quad [2]$$

322

$$323 \quad WTD_{i_{rewet B}} = WTD_i - (\overline{WTD} - \overline{WTD_{rewet A}}) \quad [3]$$

324

$$325 \quad WTD_{i_{rewet C}} = \overline{WTD_{rewet B}} + 0.5 \cdot (WTD_{i_{rewet B}} - \overline{WTD_{rewet B}}) \quad [4]$$

326

327 where  $WTD_{i_{rewet A}}$ ,  $WTD_{i_{rewet B}}$  and  $WTD_{i_{rewet C}}$  is the daily WTD in a grid cell for rewetting  
328 scenario A, B and C, respectively.  $WTD_i$  is the daily WTD in a grid cell from the calibrated hydrological  
329 model.  $\overline{WTD}$  is the long-term (34-year) mean WTD in a grid cell from the historical period of the  
330 calibrated hydrological model.  $\overline{WTD_{rewet A}}$  and  $\overline{WTD_{rewet B}}$  are long-term (34-year) mean WTD in a  
331 grid cell from the rewetting scenario A and B, respectively.

332 Bootstrapping means of future climate CO<sub>2</sub> emissions

333 We applied a bootstrap resampling approach to estimate the uncertainty in the mean values of soil  
334 CO<sub>2</sub> flux. Specifically, we resampled the means over the 17 climate models, each containing 30 annual  
335 values, with replacement. This process was repeated 10,000 times to construct bias-corrected and  
336 percentile-based 95% confidence intervals around the bootstrapped means.

337



## 338 Results

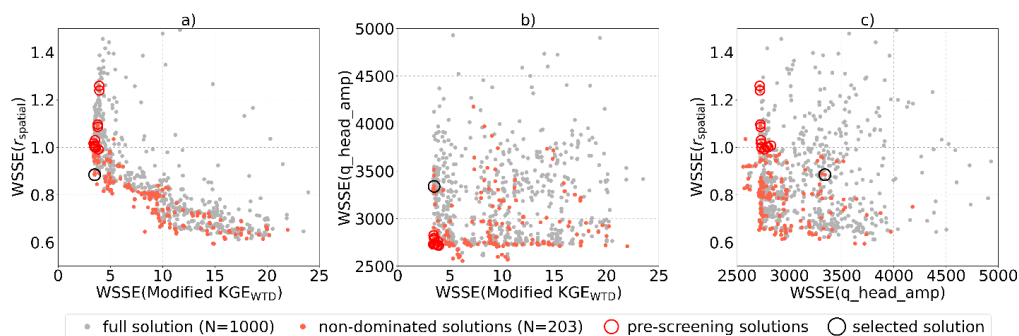
### 339 Hydrological model

#### 340 Calibration of the hydrological model

341 The model calibration, running 1000 model evaluations based on three objective function groups,  
342 using Ostrich ParaPADDs optimizer with 40 parallel model executions, took ~24 hours on a Xeon Et-  
343 4850 @2,20 GHz Server. The calibration resulted in 203 non-dominated solutions forming a three-  
344 dimensional pareto front. Figure 2 presents scatterplots of the three objective functions, illustrating  
345 the trade-offs between them. Especially, there is a clear trade-off between the two objective functions  
346 addressing temporal dynamics ( $KGE_{WTD}$ ) and spatial dynamics ( $r_{spatial}$ ), as illustrated in Figure 2a.

347 The number of non-dominated solutions and the trade-offs illustrate that several parameter sets can  
348 be considered and that an ensemble of parameter sets could be selected. For the purpose of further  
349 analysis and climate change impact assessments, however, we select one balanced solution from the  
350 non-dominated solutions, through a stepwise procedure. First, a pre-screening was performed with  
351 performance criteria for WTD of  $KGE_{WTD}$  larger than 0.6, for discharge of  $KGE_{discharge}$  larger than 0.6 and  
352 for hydraulic head in deeper wells of  $\pm 1$  m, for  $ME_{head}$  and  $ME_{amp}$ , respectively. Afterwards, the  
353 balanced parameter set was selected as the solution with the highest spatial correlation ( $r_{spatial}$ ).

354 The selection procedure was designed to prioritize accurate simulation of the temporal dynamics of  
355 peatland WTD, while maintaining strong performance across additional objective functions and  
356 maximizing spatial correlation accuracy. Initial calibration efforts indicated that achieving a  $KGE_{WTD}$   
357 value greater than 0.6 was necessary to ensure an adequate alignment between the simulated and  
358 observed WTD time series.



359

360 *Figure 2: Scatterplots of WSSE (weighted sum of squared errors) for the three objective function groups in the calibration.*  
361 *Pareto front for 1000 model evaluations.*

### 362 Hydrological model performance

363 Model performance metrics for the selected solution are summarized in Table 2. The  $q_{head\_amp}$   
364 objective function is separated into individual contributions from the metrics  $KGE_q$ ,  $ME_{head}$  and  $ME_{amp}$ .  
365 Additionally, Table 2 shows the three metrics which make up the modified  $KGE_{WTD}$ :  $r_{WTD}$ ,  $\alpha_{WTD}$  and  $ME_{WTD}$ .  
366 In general, the model performs well with a  $KGE_{WTD}$  in peat of 0.64, a  $KGE_q$  of 0.63, a  $ME_{head}$  for the deep  
367 wells of 0.75 m and a  $ME_{amp}$  for the deep wells of 0.51 m for the selected solution. However, the  
368 correlation coefficient for the spatial variability ( $r_{spatial}$ ) is poor with a value of 0.06. The model  
369 optimization achieves solid metrics on all the three components of  $KGE_{WTD}$ . The mean bias of WTD  
370 across all shallow peatland observation wells ( $ME_{WTD}$ ) is only 8 cm (Table 2).



Table 2: Hydrological model performance

Name of metric		Abbreviation	Unit	Selected solution
Modified KGE on WTD		$KGE_{WTD\text{modified}}$	-	0.64
	Correlation coefficient WTD	$r_{WTD}$	-	0.83
	Measure of variance	$\alpha_{WTD}$	-	0.14
	Mean error of WTD	$ME_{WTD}$	m	0.08
Spatial correlation of the mean WTD		$r_{\text{spatial}}$	-	0.06
KGE on discharge		$KGE_q$	-	0.63
Mean error on the hydraulic heads		$ME_{\text{head}}$	m	0.75
Mean error on amplitude of the hydraulic heads		$ME_{\text{amp}}$	m	0.51

Though the model obtains a relatively small mean error, it largely underestimates the spatial variability in WTD. The observed mean WTD variability across the 22 monitoring wells ( $SD = 16.5$  cm) is considerably higher than that observed in the simulations ( $SD = 6.8$  cm). Even though the model performance on  $KGE_{WTD}$  was generally good, it proved difficult to reproduce the spatial variation in mean WTD.

To investigate the underestimation of spatial variability in WTD, we analyzed several spatial variables considered relevant for explaining the observed variability in WTD: peat thickness, topography and proximity to water bodies. However, no clear correlation was found between these spatial variables and the mean observed WTD or model bias, as all had a correlation coefficient smaller than 0.34. See Table S6.

Historical simulations of water table depth

The simulated WTD, generated by the calibrated hydrological model driven by historical climate for the period 1990–2023, adequately represent both the observed seasonal patterns of WTD and their short-term responses to precipitation events. Figure 3 shows the time series of WTD from two individual monitoring wells as a typical example of the temporal match between observed and simulated WTD.

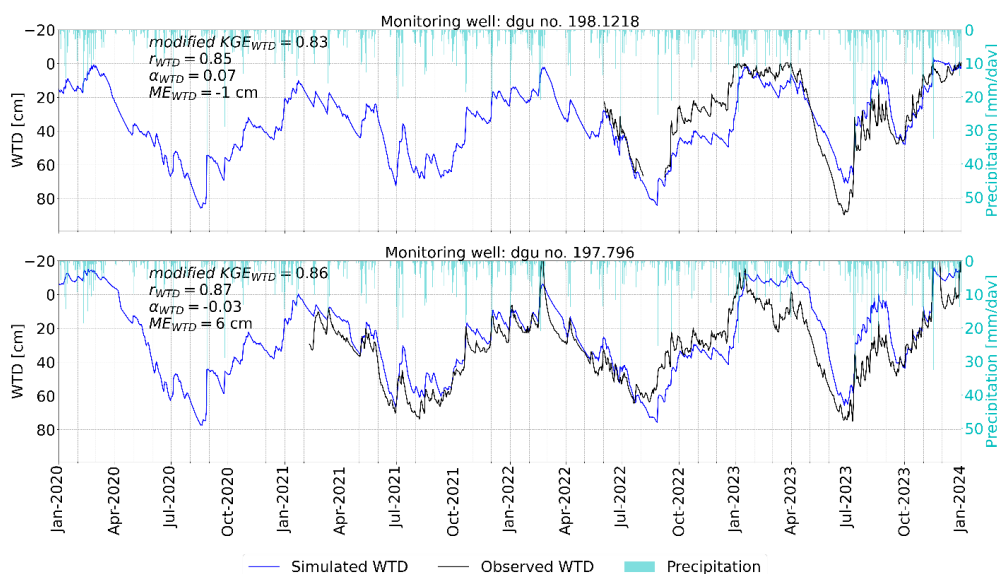


Figure 3: Example of observed and simulated timeseries for water table depth (WTD) for monitoring wells dgu no. 198.1218 and dgu no. 197.796. Including metrics for these wells.



391 Meteorological climate predictions  
392 Changes in precipitation, temperature and evapotranspiration patterns in future climate projections  
393 for Denmark generally indicate an increase in both temperature and annual precipitation. Table 3  
394 presents the mean air temperature, mean annual precipitation and mean potential evapotranspiration  
395 derived from the 17 climate projections across the three simulation periods.

396 *Table 3: Mean  $\pm$  SD (n=17) of annual air temperature, precipitation and potential evapotranspiration from the 17 climate*  
397 *models during the three simulation periods.*

	Unit	Reference period (1991-2020)	Near future (2041-2070)	Distant future (2071-2100)
Mean annual air temperature	°C	8.9 $\pm$ 0.7	10.6 $\pm$ 0.8	12.1 $\pm$ 0.8
Mean annual precipitation	mm yr <sup>-1</sup>	780 $\pm$ 121	837 $\pm$ 130	906 $\pm$ 152
Mean annual potential evapotranspiration	mm yr <sup>-1</sup>	621 $\pm$ 25	678 $\pm$ 27	727 $\pm$ 27

398

399 Hydrological climate predictions  
400 Climate simulations using the hydrological model indicate a decreasing trend in mean annual WTDs  
401 (Table 4), resulting in a shallower annual mean groundwater table in future climate conditions. Both  
402 summer and winter mean WTDs are projected to be closer to the terrain, suggesting generally wetter  
403 conditions. The mean annual amplitude of WTD remains unchanged under future climate scenarios  
404 (Table 4), indicating that there is no greater seasonal drawdown of the water table during summer,  
405 although the duration of the drawdown period may be extended.

406 *Table 4: Statistics of WTD when using the hydrological model for climate simulations. Mean  $\pm$  SD (n=17) over the 17 climate*  
407 *models during the three simulation periods. Summer is June, July and August, Winter is December, January and February. The*  
408 *amplitude is based on the monthly means of WTD to avoid outliers.*

	Unit	Reference period (1991-2020)	Near future (2041-2070)	Distant future (2071-2100)
Mean annual WTD	cm	31 $\pm$ 1	27 $\pm$ 2	24 $\pm$ 3
Mean summer WTD	cm	47 $\pm$ 1	40 $\pm$ 3	34 $\pm$ 3
Mean winter WTD	cm	18 $\pm$ 2	14 $\pm$ 4	10 $\pm$ 3
Mean annual WTD amplitude	cm	51 $\pm$ 2	50 $\pm$ 4	52 $\pm$ 4

409

410 Derivation of empirical daily soil CO<sub>2</sub> flux model  
411 An analysis of the Vejrumbrø dataset indicated a clear temperature dependency on the relation  
412 between soil CO<sub>2</sub> flux (fCO<sub>2</sub>) and WTD. The Vejrumbrø dataset was resampled to daily means of WTD,  
413 T<sub>air</sub> and soil CO<sub>2</sub> flux across the six spatial replicate measurement points omitting data from days with  
414 less than 24 flux measurements. This resulted in a dataset with 231 daily observations for each of fCO<sub>2</sub>,  
415 WTD and T<sub>air</sub> distributed evenly over a year. Traditionally, empirical emission models for ecosystem  
416 respiration (R<sub>eco</sub>) are fitted to soil temperature. However, due to the strong linear relationship  
417 between daily soil temperature and daily air temperature at the Vejrumbrø site (r = 0.96, p-value <  
418 0.001) (Figure S4), T<sub>air</sub> was used as a proxy for soil temperature when fitting the *Daily WTD-T<sub>air</sub> model*.  
419 This use of air temperature also facilitates upscaling and omits the need for projecting soil  
420 temperatures under climate change scenarios.

421 To investigate how the WTD-fCO<sub>2</sub> relation scales with temperature, we binned daily soil CO<sub>2</sub> flux into  
422 five temperature intervals: <4°C (n=39), 4-8°C (n=32), 8-12°C (n=52), 12-16°C (n=70) and >16°C (n=38)  
423 and applied a linear regression model (y=ax) with the intercept constrained at zero within each  
424 temperature bin. The regressions were constrained to pass through the origin, reflecting the  
425 assumption that soil CO<sub>2</sub> flux is zero when the WTD is zero. Thereby, the relationship between fCO<sub>2</sub>  
426 and WTD within each temperature bin was modeled using a linear regression of the form:



$$fCO_2 = a \cdot WTD \quad [5]$$

where  $fCO_2$  represents soil  $CO_2$  flux [ $Mg\ CO_2\text{-}C\ ha^{-1}\ day^{-1}$ ],  $a$  denotes the fitted slope and WTD is water table depth [cm], with positive values indicating depths below the terrain.

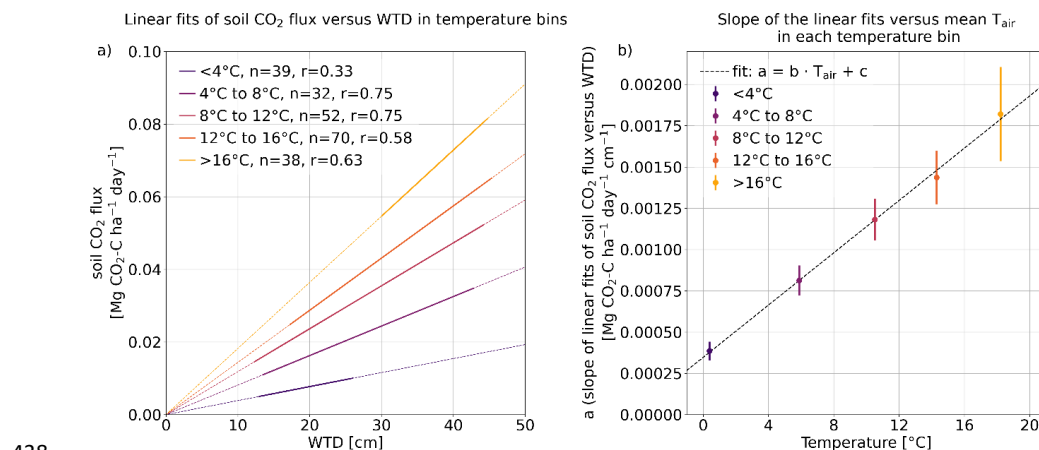
This analysis revealed an increasing slope, i.e. sensitivity of soil  $CO_2$  flux to changes in WTD, with rising temperature (Figure S5 and Figure 4a), indicating that the WTD-  $fCO_2$  slope ( $a$ ) can be modelled as a linear function of temperature ( $T_{air}$ ) (Figure 4b):

$$a = b \cdot T_{air} + c \quad [6]$$

Combining these relationships yields a simple model of the soil  $CO_2$  flux:

$$fCO_2 = b \cdot T_{air} \cdot WTD + c \cdot WTD \quad [7]$$

where  $T_{air}$  [ $^{\circ}C$ ] is the temperature,  $b$  [ $Mg\ CO_2\text{-}C\ ha^{-1}\ day^{-1}\ cm^{-1}\ ^{\circ}C^{-1}$ ] and  $c$  [ $Mg\ CO_2\text{-}C\ ha^{-1}\ day^{-1}\ cm^{-1}$ ] are empirical constants.



438

439 Figure 4: Left: linear models of soil  $CO_2$  flux vs. water table depth (WTD) in air temperature bins. The thicker segment of the  
440 line represents the range of data used to derive the fitted model.  $n$  is the number of daily observations of soil  $CO_2$  flux in each  
441 temperature bin.  $r$  is Pearson correlation coefficient. Raw data behind the linear regressions can be seen at Figure S5. Right:  
442 Slope (incl. uncertainty) (of the linear fit of soil  $CO_2$  flux versus WTD) versus observed mean temperature in each temperature  
443 bin.

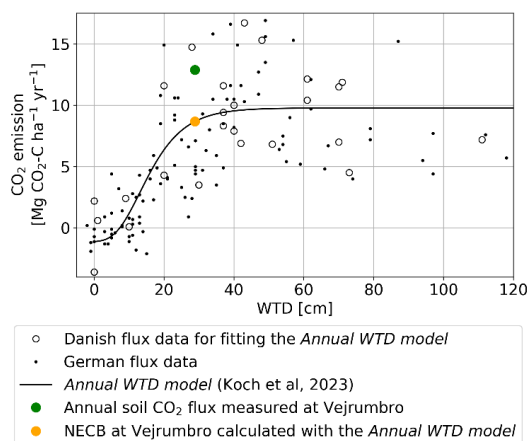
444 Having established a suitable form of the empirical soil  $CO_2$  flux equation, we used nonlinear least  
445 squares fit to estimate the  $b$  and  $c$  parameters based on the daily soil  $CO_2$  flux,  $T_{air}$  and WTD (without  
446 temperature bins). This method minimizes the residual sum of squares between the observed soil  $CO_2$   
447 flux and the *Daily WTD- $T_{air}$  model*. The resulting fitted model demonstrated a significant correlation to  
448 the observed data ( $r = 0.78$ ,  $p$ -value  $< 0.001$ ,  $RMSE = 0.021\ Mg\ CO_2\text{-}C\ ha^{-1}\ day^{-1}$ ) (Figure S6) with daily  
449 soil  $CO_2$  flux increasing in response to rising WTD and  $T_{air}$  (Figure S7). The fitted empirical constants are  
450 as follows:  $b = 8.32 \cdot 10^{-5}\ Mg\ CO_2\text{-}C\ ha^{-1}\ day^{-1}\ cm^{-1}\ ^{\circ}C^{-1}$ ,  $c = 3.33 \cdot 10^{-4}\ Mg\ CO_2\text{-}C\ ha^{-1}\ day^{-1}\ cm^{-1}$ .

451 The *Daily WTD- $T_{air}$  model* predicts the highest soil  $CO_2$  flux under conditions of simultaneously high  $T_{air}$   
452 and WTD, where a high WTD refers to a water table located furthest below the terrain (dry  
453 conditions). The multiplicative *Daily WTD- $T_{air}$  model* demonstrated a moderate fit to the soil  $CO_2$  flux  
454 data, with a  $R^2$  of 0.61. To assess the individual contributions of the predictor variables, we also  
455 computed the  $R^2$  between  $CO_2$  flux and  $T_{air}$  and WTD separately. This was done using a constructed  
456 dataset that included all combinations of WTD and  $T_{air}$  within the model range. This resulted in  $R^2$



values of 0.34 for  $T_{air}$  and 0.54 for WTD (Table S7). These values reflect the explanatory power of each variable in isolation.

Despite the significant variability in the observed net ecosystem carbon balance (NECB) used for the *Annual WTD model* (Figure 5) it is considered to represent a robust mean as it is based on multiple sites and years for Danish and German conditions. Compared to the *Annual WTD model* both the measured soil  $CO_2$  flux ( $12.9 \text{ Mg } CO_2\text{-C ha}^{-1} \text{ yr}^{-1}$  (green circle)) and the *Daily WTD- $T_{air}$*  simulated soil  $CO_2$  flux ( $13.6 \text{ Mg } CO_2\text{-C ha}^{-1} \text{ yr}^{-1}$  (not shown)) at Vejrumbro are above the corresponding fitted value of NECB ( $8.7 \text{ Mg } CO_2\text{-C ha}^{-1} \text{ yr}^{-1}$  (orange circle)) based on an annual WTD of 29 cm, but still within the range of observed NECBs used for fitting the *Annual WTD model* (Figure 5). This may be explained by the methodology of flux measurements at Vejrumbro that did not consider GPP ( $CO_2$  uptake) and therefore are expected to result in higher net  $CO_2$  fluxes. In order to align the *Daily WTD- $T_{air}$*  model to the level of the *Annual WTD model* where GPP is included, a scaling factor based on the above differences ( $f_{scaling} = 0.64$ ) was applied to equation 7 to account for lack of GPP in the soil  $CO_2$  fluxes used for empirical model development. Applying this scaling factor, we seek to avoid the risk of overestimating emissions when applying the *Daily WTD- $T_{air}$*  model at other locations.



472

473 *Figure 5: The Annual WTD model together with the Danish flux data of annual NECB and WTD data underlying the model*  
474 *(Koch et al., 2023). German flux data are included for comparison (Tiemeyer et al., 2020). Colored circles are measured and*  
475 *calculated soil  $CO_2$  flux and NECB for the Vejrumbro dataset, so the colored circles represent the year 2022-2023.*

The Vejrumbro dataset used for fitting the *Daily WTD- $T_{air}$*  model was limited to a maximum WTD of 47 cm and maximum  $T_{air}$  of  $21^\circ\text{C}$  (Figure S7). Outside of this range, the predictions of the *Daily WTD- $T_{air}$*  model exhibit increased uncertainty. It is required that the *Daily WTD- $T_{air}$*  model is sensitive to the WTD range comparable to the annual WTD variation in the *Annual WTD model*. In the *Annual WTD model*, the Annual NECB reaches 90% of its maximum asymptotic level at a mean annual WTD of 30 cm (Figure 5). The mean annual WTD results from intra-annual (within year) WTD variation. The mean annual amplitude (based on monthly means) of the observed WTD time series at the Tuse Stream catchment study site ( $n=22$ ), which is used for calibrating the hydrological model, is 65 cm. We assume that the mean annual WTD of 30 cm originates from an annual WTD variation of  $\pm$ half of that amplitude. Therefore, we assume that the WTD sensible range of the *Daily WTD- $T_{air}$*  model is  $30 + 65/2 \text{ cm} = 62.5 \text{ cm}$ . Thus, when applying the *Daily WTD- $T_{air}$*  model, daily WTD values and  $T_{air}$  values were truncated, setting WTD and  $T_{air}$  to 62.5 cm and  $25^\circ\text{C}$ , respectively, when exceeding those thresholds.

In both the *Daily WTD- $T_{air}$*  model and the *Annual WTD model*,  $CO_2$  fluxes are constrained so that the model does not simulate negative fluxes or carbon uptake. Thus, both  $CO_2$  flux models exclusively





490 account for the CO<sub>2</sub> emissions from the peat soil, without representing its potential role as a carbon  
491 sink (Gyldenkerne et al., 2025).

492 CO<sub>2</sub> emissions from peatlands

493 CO<sub>2</sub> emissions throughout the historical simulation period

494 The long-term mean of the emission factor for the Tuse Stream catchment peat area is  $8.0 \pm 0.8$  Mg

495 CO<sub>2</sub>-C ha<sup>-1</sup> yr<sup>-1</sup> (mean  $\pm$  SD, n=34) when using the *Annual WTD model* and  $8.8 \pm 1.6$  Mg CO<sub>2</sub>-C ha<sup>-1</sup> yr<sup>-1</sup>

496 (mean  $\pm$  SD, n=34) when using the *Daily WTD-T<sub>air</sub> model* (Table 5).

497 *Table 5: Long-term mean water table depth (WTD), long-term mean annual WTD amplitude (based on monthly means of WTD*  
498 *to avoid outliers) and long-term soil CO<sub>2</sub> flux, throughout the historical period and the three modified 34-year WTD time series*  
499 *of rewetting scenarios. Mean  $\pm$  SD is based on the 34 years of the historical period (1990-2023).*

	Unit	Historical period (1990-2023)	Rewetting scenario A	Rewetting scenario B	Rewetting scenario C
Mean WTD	cm	34 $\pm$ 8	14 $\pm$ 18	14 $\pm$ 8	14 $\pm$ 4
Mean annual WTD amplitude	cm	51 $\pm$ 11	110 $\pm$ 28	51 $\pm$ 11	26 $\pm$ 5
CO <sub>2</sub> emission from <i>Daily WTD-T<sub>air</sub> model</i> aggregated to annual	Mg CO <sub>2</sub> -C ha <sup>-1</sup> yr <sup>-1</sup>	8.8 $\pm$ 1.6	7.7 $\pm$ 2.0	5.2 $\pm$ 1.5	4.4 $\pm$ 0.8
CO <sub>2</sub> emission from <i>Annual WTD model</i> aggregated to annual	Mg CO <sub>2</sub> -C ha <sup>-1</sup> yr <sup>-1</sup>	8.0 $\pm$ 0.8	4.6 $\pm$ 3.0	4.3 $\pm$ 2.0	4.4 $\pm$ 1.2

500

501 Figure 6 shows T<sub>air</sub>, as wells as the spatial mean of WTD and CO<sub>2</sub> emissions across the peatland, as  
502 simulated by the *Daily WTD-T<sub>air</sub> model* and the *Annual WTD model* during the historical period. The  
503 CO<sub>2</sub> emissions calculated with the *Daily WTD-T<sub>air</sub> model* (red line in Figure 6c, 6d) depend on both the  
504 observed daily temperature variability (orange line in Figure 6a) and simulated intra-annual (seasonal)  
505 WTD variability (blue line in Figure 6b), while the CO<sub>2</sub> emission calculated with the *Annual WTD model*  
506 (black points in Figure 6d) only depends on the inter-annual (annual means) WTD (blue points in Figure  
507 6b) and not the temperature.

508 Inter-annual (between years) variation in CO<sub>2</sub> emission is substantially larger when using the *Daily*  
509 *WTD-T<sub>air</sub> model* (SD = 1.6 Mg C-CO<sub>2</sub> ha<sup>-1</sup> yr<sup>-1</sup>) compared to the *Annual WTD model* (SD = 0.8 Mg C-CO<sub>2</sub>  
510 ha<sup>-1</sup> yr<sup>-1</sup>) (Figure 6d), as the former captures extreme events, such as periods of high temperature or  
511 deep groundwater tables, as well as compound events involving the simultaneous occurrence of both.  
512 In contrast, the *Annual WTD model* is insensitive to temperature and the intra-annual (within year)  
513 timing of deep WTD. Moreover, the *Annual WTD model* imposes an upper limit of 10 Mg CO<sub>2</sub>-C ha<sup>-1</sup>  
514 yr<sup>-1</sup> for annual emissions (Koch et al., 2023) (Figure 5). During the summer of 2018, a compound  
515 extreme event occurred, characterized by both high temperatures and deep groundwater table. The  
516 annual CO<sub>2</sub> flux for this year shows a 34% increase when estimated using the *Daily WTD-T<sub>air</sub> model*  
517 compared to the *Annual WTD model*. This discrepancy arises from the *Daily WTD-T<sub>air</sub> model's* ability to  
518 account for the prolonged duration of concurrent high temperatures and deep groundwater table  
519 conditions throughout the summer (Figure 6d). Conversely, in 2010, the *Daily WTD-T<sub>air</sub> model*  
520 estimates significantly lower annual CO<sub>2</sub> emissions compared to the *Annual WTD model* (Figure 6d).  
521 This difference is due to the emission model's ability to account for the effects of prolonged periods of  
522 low temperatures during the autumn and spring of 2010, leading to a mean annual temperature below  
523 the long-term mean, despite summer temperatures being consistent with other years (Figure 6a).  
524 Examples of years with extreme events primarily driven by either WTD or T<sub>air</sub> include 1996, which  
525 experienced a significant summer decline in groundwater table (Figure 6b), and 1997, which was  
526 characterized by elevated summer temperatures (Figure 6a). However, neither of these events led to



CO<sub>2</sub> emissions as high as those simulated during the compound event of both high temperatures and deep water table in 2018 (Figure 6).

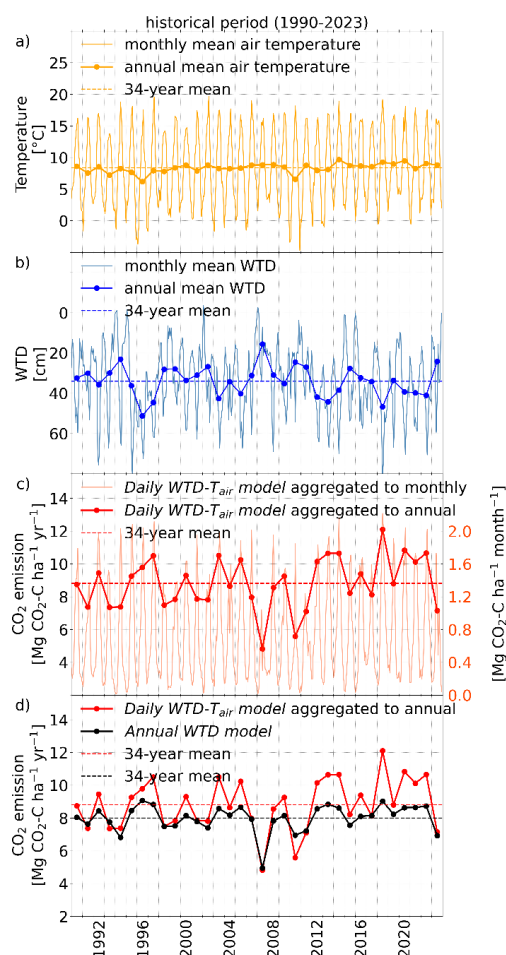


Figure 6: Air temperature ( $T_{air}$ ), water table depth (WTD) and soil CO<sub>2</sub> emission for the historical simulation period 1990-2023.

CO<sub>2</sub> emissions under different rewetting scenarios

The rewetting scenarios represent an adjustment to the WTD simulated by the hydrological model over the 34-year historical period, thereby reflecting the climatological conditions prevailing during that time. Across all three rewetting scenarios, the long-term (34-year) mean WTD was raised by 20 cm, from 34 cm to 14 cm below the terrain, ensuring a consistent long-term annual mean WTD among the rewetting scenarios (Table 5). Accordingly, the application of the *Annual WTD model* for estimating CO<sub>2</sub> fluxes result in CO<sub>2</sub> emissions between  $4.3 \pm 1.2$  Mg C-CO<sub>2</sub> ha<sup>-1</sup> yr<sup>-1</sup> (mean  $\pm$  SD, n=34) and  $4.6 \pm 3.0$  Mg C-CO<sub>2</sub> ha<sup>-1</sup> yr<sup>-1</sup> (mean  $\pm$  SD, n=34) across all rewetting scenarios (Table 5). The mean annual soil CO<sub>2</sub> flux from the three rewetting scenarios, as calculated using the *Annual WTD model*, are similar but not identical. This is because the *Annual WTD model* is applied to each of the 34 individual annual mean WTD values rather than to a single long-term mean WTD. The SD of CO<sub>2</sub> emissions calculated using the *Annual WTD model* in scenario C is markedly lower than in rewetting scenario A and B, reflecting the

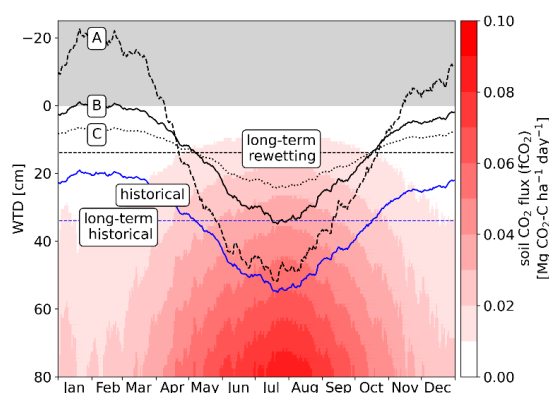


543 lower inter-annual (between years) variability in mean annual WTD observed for this scenario (Table  
544 5).

545 In contrast to the *Annual WTD model*, the *Daily WTD- $T_{air}$  model* captures the simultaneous occurrence  
546 of low groundwater table and high  $T_{air}$  during the summer months. Application of this emission model  
547 indicates that raising the groundwater table during summer months (rewetting scenario C) yields the  
548 greatest reduction potential in soil  $\text{CO}_2$  emissions (Table 5), leading to a 50% decrease in the mean  
549 value, from  $8.8 \pm 1.6$  to  $4.4 \pm 0.8 \text{ Mg C-CO}_2 \text{ ha}^{-1} \text{ yr}^{-1}$  (mean  $\pm$  SD,  $n=34$ ) (Table 5). In contrast,  
550 management scenarios that primarily target increase in winter water table (rewetting scenario A)  
551 exhibit only marginal emission reduction potential (Table 5).

552 A visual representation of daily soil  $\text{CO}_2$  emissions in relation to mean daily temperature during the 34-  
553 year historical period under different WTD conditions (Figure 7) reveals that high summer  
554 temperatures are a key driver of  $\text{CO}_2$  emissions. WTD observations from the Tuse catchment peatland  
555 indicate that, during shorter periods in the warm summer months, the WTD can exceed 80 cm (Figure  
556 3). These periods with very low summer water table contribute substantially to total  $\text{CO}_2$  emissions  
557 (Figure 7).

558 A rewetting scenario that mainly generates wetter winter conditions (rewetting scenario A) has very  
559 limited  $\text{CO}_2$  emission reduction. All three scenarios assume that even under rewetting, the peatland  
560 WTD will follow a climate driven seasonality and that obtaining zero WTD in summer periods will be  
561 difficult by classical nature-based solutions. Rewetting scenario C, which features the greatest increase  
562 in summer WTD, achieves the largest reduction in  $\text{CO}_2$  emissions (Figure 7). Permanent wet conditions  
563 with WTD at zero would be required to obtain zero  $\text{CO}_2$  emission with the developed *Daily WTD- $T_{air}$*   
564 *model*, but under such conditions, methane emissions would also come into play and plant growth  
565 would be severely limited.



566

567 *Figure 7: Colormap: Visual representation of the annual distribution of daily surface soil  $\text{CO}_2$  flux ( $f\text{CO}_2$ ,  $\text{CO}_2$  exchange with*  
568 *atmosphere) under mean daily temperature during the historical period (1990-2023) and for different water table depths*  
569 *(WTD). Curves: solid blue line: simulated daily mean WTD during the historical period and corresponding long-term (34-year)*  
570 *mean WTD, black lines: daily mean WTD for each of the modified 34-year WTD time series of rewetting scenarios (A, B and C)*  
571 *and the corresponding long-term (34-year) mean WTD.*

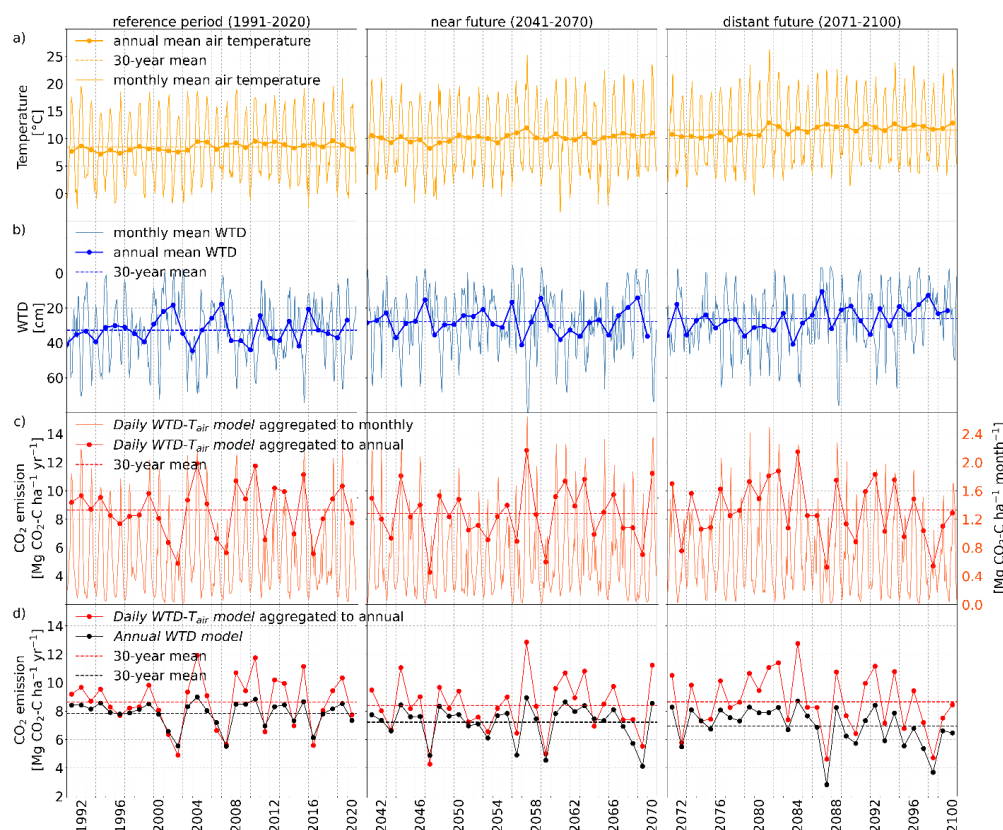
572  $\text{CO}_2$  emissions across future climate simulation periods

573 Figure 8 shows the same variables as Figure 6 but based on a representative climate model simulation  
574 instead of the observed climate record, offering a typical example of the development of temperature,  
575 WTD and soil  $\text{CO}_2$  flux through the reference, near and distant future periods based on the RCP 8.5  
576 pathway.



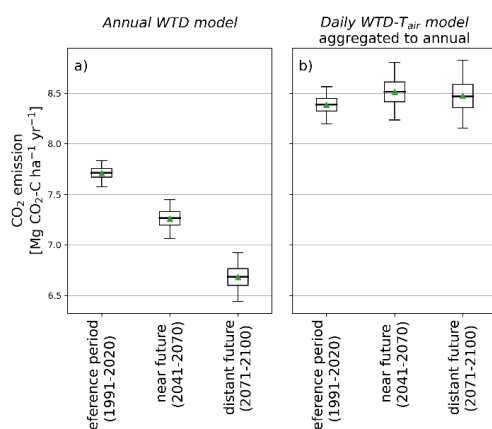
577 The future climate simulations show an increase in both the annual mean temperature and  
578 groundwater levels combined with higher maximum summer temperature (Figure 8a, 8b, Table 3,  
579 Table 4). The bootstrap mean of soil CO<sub>2</sub> flux calculated with the *Annual WTD model* over all climate  
580 models predicts a decreasing trend in soil CO<sub>2</sub> flux under future climate conditions (Figure 9a,  
581 horizontal dotted black line in Figure 8d), driven by an inter-annual (between years) mean WTD closer  
582 to terrain (Table 4, Figure 8b). However, this decreasing trend is countered by the inclusion of T<sub>air</sub>  
583 effects when applying the *Daily WTD-T<sub>air</sub> model* (Figure 9b, horizontal dotted red line in Figure 8c and  
584 8d).

585 The wider confidence intervals in the mean annual CO<sub>2</sub> emissions for the future periods with both CO<sub>2</sub>  
586 emission model (Figure 9) indicate that the inter-annual (between years) soil CO<sub>2</sub> fluxes become more  
587 variable in future climate. Furthermore, the confidence intervals for the individual periods are wider  
588 for the *Daily WTD-T<sub>air</sub>* (Figure 9b) compared to the *Annual WTD model* (Figure 9a), which is expected as  
589 variations in T<sub>air</sub> and not only WTD is included as with the *Daily WTD-T<sub>air</sub> model*. This demonstrates that  
590 the *Daily WTD-T<sub>air</sub> model* captures extreme events, including periods of high temperature or deep  
591 groundwater table, whether these events occur simultaneously (compound event) or independently.



592

593 **Figure 8:** Example of air temperature ( $T_{air}$ ), water table depth (WTD) and soil CO<sub>2</sub> flux for future climate simulation with  
594 climate model projection no. 5 (Table S6).



595

596 *Figure 9: Boxplot showing the distribution of bootstrap means of soil CO<sub>2</sub> emissions according to the Daily WTD-T<sub>air</sub> model and*  
597 *Annual WTD model during future climate. Green triangles and horizontal lines indicate the mean and the median of the*  
598 *bootstrap mean, respectively. Boxes show the 25<sup>th</sup> and 75<sup>th</sup> percentiles. Whiskers indicate the 95% confidence intervals.*  
599 *Outliers are not shown.*

600 The results presented in Figure 9 suggest that the impact on CO<sub>2</sub> emissions caused by future increases  
601 in T<sub>air</sub> and increases in water tables cancel each other out when using the *Daily WTD-T<sub>air</sub> model*. To  
602 investigate this further, we analyze how the combination of T<sub>air</sub> and WTD shift between the reference  
603 and the distant future periods, despite relatively stable total CO<sub>2</sub> emission.

604 We wish to identify the specific combination of T<sub>air</sub> and WTD that are associated with the majority of  
605 the CO<sub>2</sub> emission. Due to the non-linear response of soil CO<sub>2</sub> flux to environmental drivers in the *Daily*  
606 *WTD-T<sub>air</sub> model*, a large fraction of total emissions is generated on relatively few days. To quantify this,  
607 we calculated p50, defined as the proportion of days required to account for 50% of the total annual  
608 soil CO<sub>2</sub> flux (fCO<sub>2</sub>). This was achieved by ranking the daily values of fCO<sub>2</sub>, WTD, and T<sub>air</sub> in ascending  
609 order according to fCO<sub>2</sub>. Subsequently, the ranked fCO<sub>2</sub> values were cumulatively summed to obtain  
610 their percentile distribution (Figure S8). The procedure was first applied to fCO<sub>2</sub>, WTD, and T<sub>air</sub> data  
611 from the historical simulation period, with the resulting percentile curves shown in Figure S8. Over the  
612 historical simulation period, 50% of the total fCO<sub>2</sub> (fCO<sub>2, p50</sub>) was generated within 22% of the days (p50  
613 = 22%), while the value of fCO<sub>2, p50</sub> and corresponding WTD<sub>p50</sub> and T<sub>air, p50</sub> are estimated to be 4.15·10<sup>-2</sup>  
614 g CO<sub>2</sub>-C ha<sup>-1</sup> day<sup>-1</sup>, 47 cm and 13.8 °C (Table 6 and Figure S8).

615 Similar estimates are derived from the three timeslots from the climate models (reference, near- and  
616 distant future) using the 17 different climate models. For the future, 50% of the total fCO<sub>2</sub> is expected  
617 to occur within approximately 21 ± 1 % (mean ± SD, n=17) of the days (Table 6). The daily soil CO<sub>2</sub> flux  
618 associated to p50 (fCO<sub>2, p50</sub>) and p50 are nearly identical across both the historical and future climate  
619 simulations periods (Table 6). As also shown in Figure 9b, the magnitude and temporal distribution of  
620 fCO<sub>2</sub> are predicted to remain unchanged in the future. While the value of fCO<sub>2, p50</sub> remains relatively  
621 constant around 4·10<sup>-2</sup> Mg CO<sub>2</sub>-C ha<sup>-1</sup> day<sup>-1</sup> for future climate periods, the corresponding WTD<sub>p50</sub> and  
622 T<sub>air, p50</sub> values change as a result of changing climate moving towards higher temperatures (17 °C) and  
623 shallower groundwater table (40 cm).

624 Figure 10 provides a graphical representation of fCO<sub>2</sub> obtained from the *Daily WTD-T<sub>air</sub> model*, with the  
625 colormap illustrating the daily fCO<sub>2</sub> corresponding to different combinations of T<sub>air</sub> and WTD. The daily  
626 fCO<sub>2, p50</sub> (4.15·10<sup>-2</sup> g CO<sub>2</sub>-C ha<sup>-1</sup> day<sup>-1</sup> for the historical period (Table 6)) can be achieved through  
627 various combinations of T<sub>air</sub> and WTD (dark red dotted line in Figure 10). The values of T<sub>air, p50</sub> and



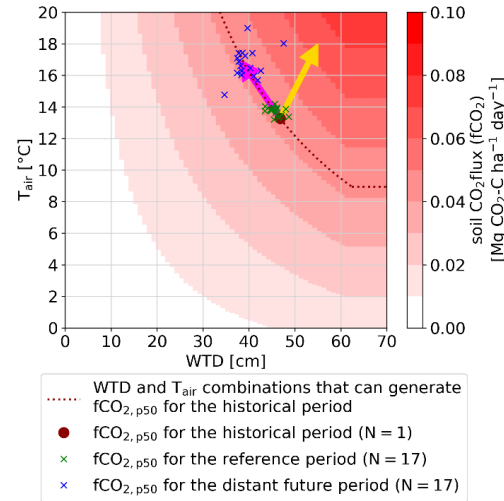
WTD<sub>p50</sub> corresponding to fCO<sub>2, p50</sub> for the Tuse Stream catchment peatland are plotted as a dark red point. As expected, the fCO<sub>2, p50</sub> values for the reference periods of the 17 climate models (green crosses at Figure 10) are closely aligned with that of the historical period. It is evident that the fCO<sub>2, p50</sub> values for the distant future climate conditions (blue crosses at Figure 10) shift along the direction indicated by the pink arrow (along the red dotted line), reflecting a trend toward higher temperatures and lower WTD (i.e. water levels closer to the terrain surface). This indicates that the mean daily fCO<sub>2</sub> (Table 6) and the long-term fCO<sub>2</sub> remains constant in the future (Figure 9b), as a result of a counterbalance between impacts of rising temperatures and rising groundwater levels.

The pink arrow at Figure 10 illustrates the characteristic impact of climate change in Denmark, reflecting the concurrent increase in air temperature and shallow groundwater levels (Schneider et al., 2022). In contrast, other regions in Europe are experiencing declining groundwater level trends to climate change (Wunsch et al., 2022). Consequently, CO<sub>2</sub> emissions from peatlands in these regions are expected to shift in the direction indicated by the yellow arrow in Figure 10, towards considerably larger emission rates.

Table 6: p50 is the fraction of days required to reach 50% of the total soil CO<sub>2</sub> flux (fCO<sub>2</sub>). fCO<sub>2, p50</sub> is the daily soil CO<sub>2</sub> flux associated with p50. WTD<sub>p50</sub> and T<sub>air, p50</sub> are the water table depth (WTD) and air temperature (T<sub>air</sub>) corresponding to fCO<sub>2, p50</sub>, respectively. Mean ± SD is based on 17 climate model simulations.

		Historical simulation period	Climate simulation periods		
	Unit	(1990-2023)	Reference period (1991-2020)	Near future (2041-2070)	Distant future (2071-2100)
p50	% days	22	21 ± 1	21 ± 1	21 ± 1
fCO <sub>2, p50</sub>	Mg CO <sub>2</sub> -C ha <sup>-1</sup> day <sup>-1</sup>	4.15·10 <sup>-2</sup>	4.03·10 <sup>-2</sup> ± 9.89·10 <sup>-4</sup>	4.00·10 <sup>-2</sup> ± 3.24·10 <sup>-3</sup>	4.03·10 <sup>-2</sup> ± 3.65·10 <sup>-3</sup>
T <sub>air, p50</sub>	°C	13.8	14 ± 0.3	15 ± 0.6	17 ± 1.0
WTD <sub>p50</sub>	cm	47	46 ± 1	42 ± 3	40 ± 3

645



646

Figure 10: Colormap: Visual representation of the Daily WTD-T<sub>air</sub> model output, illustrating soil CO<sub>2</sub> flux (fCO<sub>2</sub>) as function of daily water table depth (WTD) and air temperature (T<sub>air</sub>). The dark red dotted line represents combinations of T<sub>air</sub> and WTD that corresponds fCO<sub>2</sub> at p50 (fCO<sub>2, p50</sub>), where p50 is the fraction of days required to reach 50% of the total accumulated fCO<sub>2</sub> during the historical period. Green crosses are fCO<sub>2, p50</sub> for the reference period of the 17 climate simulations. Purple crosses are fCO<sub>2, p50</sub> for the distant future period of the 17 climate simulations. The pink and yellow arrows indicate different future trends in T<sub>air</sub> and WTD and the associated trend in CO<sub>2</sub> emissions under climate change. Specific to Denmark, the pink arrow





653 indicates increases in  $T_{air}$  and decrease in WTD, other regions might experience increase in both  $T_{air}$  and WTD and an  
654 associated large increase in  $CO_2$  emissions (yellow arrow).



## 655 Discussion

656 Peatland management under changing climate

657 In 2023, CO<sub>2</sub> emissions from drained organic soils in croplands and grasslands was estimated to  
658 accounted for 6.7% of Denmark's total emissions, including those from the Land Use, Land-Use Change  
659 and Forestry (LULUCF) sector (Nielsen et al., 2025b). Returning peatland organic soils to their natural  
660 hydrological state is a cost-effective GHG reduction strategy (IPCC, 2014; Kirpotin et al., 2021;  
661 Tanneberger et al., 2021; Wilson et al., 2016). Therefore, national policies (Regeringen, 2024) and the  
662 European Union's Nature Restoration Law (Regulation (EU) 2024/1991, 2024) seek to improve the  
663 management of peatlands and achieve climate neutrality targets under the urgent Green Transition  
664 agenda. To mitigate agricultural GHG emissions Danish ministerial agreements were initiated in 2024,  
665 targeting the restoration of 140,000 hectares of peatland (Regeringen, 2024). However, there is a need  
666 to strengthen the scientific evidence for mitigation measures to facilitate cost-effective policies.  
667 Quantitative predictions of fluxes such as the numbers presented in this study, supports prioritization  
668 and design of peatland rewetting strategies by estimating their CO<sub>2</sub> emission reduction potentials  
669 accounting for future climate variability impact on CO<sub>2</sub> emissions.

670 Integration of the process-based hydrological model of the Tuse Stream catchment with the  
671 empirically derived *Daily WTD-T<sub>air</sub> model* of soil CO<sub>2</sub> flux developed in this study revealed that emission  
672 simulations at daily timesteps produce greater variability in soil CO<sub>2</sub> fluxes compared to emission  
673 estimates derived from annual WTD means. This increased variability is attributed to the daily model's  
674 ability to account for short-term compound events, especially the simultaneous occurrence of elevated  
675 air temperatures and low groundwater levels.

676 More importantly, incorporating temperature dependence and higher temporal resolution into the  
677 CO<sub>2</sub> emissions model significantly alters the projected trends of CO<sub>2</sub> emission under both rewetting  
678 and changing climate conditions. The rewetting analyzed in this study showed how different rewetting  
679 scenarios with varying seasonal amplitudes in WTD suggest significantly different emission reduction  
680 potential even with identical annual mean WTD. The results illustrate that increasing the groundwater  
681 table during warm periods is key to obtaining CO<sub>2</sub> emission reductions, whereas rewetting strategies  
682 that mainly raise winter water table without significantly affecting the summer levels offer limited  
683 mitigation benefits. This highlights the importance of not only targeting annual reductions in WTD but  
684 particularly designing rewetting strategies to increase the summer water table and avoid critically low  
685 water levels during droughts and warm periods. Achieving such rewetted conditions may include  
686 larger forced control of WTD than what is currently being practiced for most existing rewetting  
687 schemes, where the WTD remain subject to climate seasonality impact. With such nature-based  
688 solutions it is not likely to reduce CO<sub>2</sub> emissions to the degree that current emission reduction policies  
689 target.

690 Also, projections of CO<sub>2</sub> emissions under different climate change scenarios were altered greatly by  
691 introducing temperature sensitivity and enhanced temporal resolution into the CO<sub>2</sub> emissions  
692 modeling framework. Here our results show that, while the projected rise in groundwater tables in  
693 isolation would lead to lower CO<sub>2</sub> emissions in future (when using the *Annual WTD model*), the *Daily*  
694 *WTD-T<sub>air</sub> model* revealed that anticipated increases in T<sub>air</sub> are likely to cancel out these reductions,  
695 resulting in CO<sub>2</sub> emissions on a level comparable to current levels. This is an important finding, since it  
696 suggests that increasing temperatures alone will likely increase CO<sub>2</sub> emissions, and that water level rise  
697 driven by climate change or rewetting initiatives might just counteract this trend. Rewetting measures  
698 would need to be substantially intensified to ensure climate resilience and achieve meaningful  
699 reductions in CO<sub>2</sub> emissions. Additionally, outside the specific case of Danish peatlands located in a  
700 region that is susceptible to a future wetter climate, other regions might project both increasing



temperatures and lower groundwater tables, and in such cases climate change will significantly increase emissions without any rewetting.

Hydrological simulation of groundwater levels in peat soil with process-based models Existing large scale CO<sub>2</sub> emission estimates, such as national inventories from organic soils (Gyldenkerne et al., 2025; Nielsen et al., 2025b), typically combine empirical emission models and data-driven ML approaches for estimating annual WTD (Bechtold et al., 2014; Koch et al., 2023; Tiemeyer et al., 2020). These approaches appear robust and suited for upscaling but are limited in their ability to represent the impact of sub-annual variability in temperature and WTD, which are issues that become increasingly important when analyzing effects of rewetting and climate change. In contrast to most data-driven approaches, hydrological models enable a climate-driven representation of WTD temporal dynamics and the underlying hydrological processes. Moreover, the use of physically based models has the distinct advantage of enabling scenario-based analyses, such as the evaluation of alternative land use strategies and the projection of future hydrological conditions under climate change scenarios. Utilizing hydrological models that generate high-resolution time series of WTD, it is possible to quantify impacts of WTD dynamics, including water levels, temporal variability and seasonal amplitudes, on changes in CO<sub>2</sub> emissions.

A unique feature of the present study is that the hydrological model of Tuse Stream catchment is developed in the same modelling framework as the National Hydrological Model of Denmark (Henriksen et al., 2020; Stisen et al., 2019). The National Hydrological Model is continuously updated with new data and operates in near real-time. This integration enables a link between the lessons learned from the Tuse Stream catchment-scale model and the National Hydrological Model of Denmark, thereby improving the representation of peatland hydrology and contributing to the refinement of future national GHG inventories.

As a continuation of this study, we will further investigate the spatial variability of WTD and extent hydrological model to include additional peatland-dominated catchments. Additionally, we will utilize the National Hydrological model to simulate WTD across all Danish peatlands.

Selection, fit and transferability of daily CO<sub>2</sub> emission model A range of empirical models with varying levels of complexity has been developed to describe ecosystem respiration; however, the most commonly applied formulation is the Lloyd–Taylor model (Lloyd J., Taylor, 1994), in which temperature acts as the sole independent variable. Structural complexity in empirical equations is increased through the integration of various other environmental variables, for example, hydrological variables such as WTD (Rigney et al., 2018).

To evaluate alternative empirical emission models alongside our *Daily WTD-T<sub>air</sub> model*, we fitted three different empirical formulations from Rigney et al. (2018) to the Vejrumbro soil CO<sub>2</sub> flux data (Table S7). Each of the three empirical formulations incorporated both temperature and WTD as independent variable. The model fitting resulted in R<sup>2</sup> values comparable to those obtained from fitting the *Daily WTD-T<sub>air</sub> model* developed in this study (Table S7).

Studying the explanatory power of each independent variable of WTD and T<sub>air</sub> in isolation in the other empirical emission models, revealed that models in which WTD and T<sub>air</sub> are incorporated as additive terms, rather than as interdependent (e.g., multiplicative) terms (as in eq. 6 and 8 in Rigney et al., (2018)), often exhibit coefficients of determination (R<sup>2</sup>) that are excessively dominated by either WTD or T<sub>air</sub> (Table S7). This indicates that such model formulations may inadequately capture the joint or synergistic effects of these variables on the dependent variable. The challenge likely stems from the fact that both WTD and T<sub>air</sub> exhibit similar seasonal patterns, which may lead the regression to primarily fit one of the additive terms containing either WTD or T<sub>air</sub>. Empirical models that incorporate



746 WTD and  $T_{air}$  as multiplicative terms (such as equation 7 in Rigney et al. (2018) and the *Daily WTD- $T_{air}$*   
747 model developed in this study) demonstrate a more balanced distribution of explanatory power  
748 between each independent variable (Table S7). Nevertheless, equation [7] in Rigney et al. (2018)  
749 remains predominantly influenced by the  $T_{air}$  component (Table S7). A more balanced distribution of  
750 explanatory power between temperature and WTD is desirable, given that both variables are  
751 recognized as key drivers of soil  $CO_2$  flux dynamics, which is achieved better with the *Daily WTD- $T_{air}$*   
752 than with any of the empirical models in Table S7.

753 In this study, we demonstrate the need for the development of emission models operating on a sub-  
754 annual timescale. It highlights the necessity of creating scalable generalized models based on  
755 temperature, WTD and possibly other predictors. The development of such models requires data from  
756 a large number of sites with continuous and temporally dense measurement, in order to integrate  
757 information in a manner similar to models based on annual WTD. We recognize that currently, models  
758 based on annual WTD are likely the most robust for upscaling to national level and current conditions.

759 The simulated soil  $CO_2$  flux at Vejrumbro, estimated using the *Daily WTD- $T_{air}$*  model ( $13.6 \text{ Mg } CO_2\text{-C ha}^{-1}$   
760  $\text{yr}^{-1}$ ), aligns well with flux measurements from Danish and German sites (Figure 5). This agreement  
761 suggests a comparable magnitude of emissions across geographically distinct locations of similar  
762 characteristics, such as soil type and land use history.

763 We acknowledge that the *Daily WTD- $T_{air}$*  model is derived from a single dataset, and that other  
764 emission models also provide valid fits of WTD and  $T_{air}$ . Furthermore, we recognize that empirical  
765 emission models are highly dependent on the specific data to which they are fitted. Acknowledging the  
766 limited data behind the *Daily WTD- $T_{air}$*  model utilized in this study, the goal has not been to accurately  
767 estimate the peatland emission budget, which will be uncertain due to the reliance on a single site.  
768 However, the objective has been to illustrate the impact and insights gained from applying emission  
769 models at a daily timescale and how this has significant impact on the conclusions that can be made  
770 regarding effects of rewetting and climate change. The decision to utilize the *Daily WTD- $T_{air}$*  model for  
771 rewetting and climate modeling scenarios is motivated by the simplicity of the relationship and its  
772 direct derivation from the Vejrumbro data, which clearly demonstrates a temperature-dependent  
773 relationship between soil  $CO_2$  flux and WTD. The limited availability of multiple high-temporal-  
774 resolution GHG emission datasets broadly restricts the ability to generalize and upscale empirical GHG  
775 emission models at a daily timescale. Therefore, we consider the *Daily WTD- $T_{air}$*  model to be the most  
776 reliable option currently available. Future research should validate the performance of emission  
777 models on intra-annual (within years) data with continuous measured  $CO_2$  data.

778 A promising methodology for future applications, as well as for integrating a Tier 3 framework,  
779 involves coupling a process-based hydrological model with process-based emission models or an  
780 empirically derived daily emission model, such as the one developed in this study, to enable detailed  
781 simulations of GHG emissions that capture short-term dynamics and compound environmental effects.

782

783



## 784 Conclusion

785 This study demonstrates the feasibility of simulating the temporal dynamics of the peatland water  
786 balance and shallow groundwater table depth (WTD) using a catchment-scale distributed hydrological  
787 model. Accurately modelling shallow WTD is critical for reliable projections of CO<sub>2</sub> emissions from  
788 peatlands. We combined simulations of shallow WTD from the calibrated hydrological model with two  
789 empirical CO<sub>2</sub> emission models 1) an annual WTD-CO<sub>2</sub> relationship and 2) a daily WTD-CO<sub>2</sub> model  
790 accounting for the temperature effect on soil CO<sub>2</sub> production. This approach was used to estimate net  
791 soil CO<sub>2</sub> emissions for the historical period (1991-2020), the near future (2041-2070) and the distant  
792 future (2071-2100). This demonstrated that projections of soil CO<sub>2</sub> emissions are highly sensitive to the  
793 complexity and temporal resolution of the emission model applied. Specifically, models that  
794 incorporate both temperature and WTD dynamics at a daily timescale results in vastly different  
795 conclusion regarding impacts of climate change and rewetting. Regarding climate change impacts, we  
796 show that a daily temperature and WTD based emission model predict increased emissions due to  
797 temperature changes, which can be counter balanced (in the Danish case) or amplified depending on  
798 the future trend in WTD. Our results also demonstrate that rewetting strategies aimed at raising the  
799 groundwater table during the warm summer period offer a CO<sub>2</sub> emission reduction potential of up to  
800 50%, whereas approaches focused primarily on increasing winter water table levels result in only  
801 marginal reductions. The combination of process-based hydrological model simulations and a daily-  
802 resolution empirical CO<sub>2</sub> emission model used in this study captures the influence of short-term  
803 compound climate events—such as simultaneous high temperatures and low WTD—which  
804 substantially alters projected emission trends compared to simpler approaches. Such refined  
805 approaches are essential for developing adaptive, climate-resilient peatland restoration policies and  
806 improving national greenhouse gas inventories. The findings underscore the importance of moving  
807 beyond static, annual WTD thresholds in peatland management by incorporating dynamic hydrological  
808 simulations. Instead, rewetting strategies should prioritize maintaining elevated summer groundwater  
809 table levels to buffer against drought-induced emission peaks.

## 810 Supplement link

811 ...

## 812 Author contributions

813 All authors contributed to the conception and design of the study. TD conducted the analysis and  
814 drafted the manuscript, with input and revisions from all co-authors.

## 815 Competing interests

816 The authors declare that they have no conflict of interest.

## 817 Acknowledgements

818 We would like to thank Independent Research Fund Denmark for supporting the project PEATlands and  
819 Climate-driven variability in groundwater depth – Impacts on greenhouse gas Emissions.

## 820 References

821 Adhikari, K., Hartemink, A. E., Minasny, B., Bou Kheir, R., Greve, M. B., and Greve, M. H.: Digital  
822 mapping of soil organic carbon contents and stocks in Denmark, PLoS One, 9,  
823 <https://doi.org/10.1371/journal.pone.0105519>, 2014.

824 Ala-aho, P., Soulsby, C., Wang, H., and Tetzlaff, D.: Integrated surface-subsurface model to investigate



- 825 the role of groundwater in headwater catchment runoff generation: A minimalist approach to  
826 parameterisation, *J. Hydrol.*, 547, 664–677, <https://doi.org/10.1016/j.jhydrol.2017.02.023>, 2017.
- 827 Arents, E. J. M. M., van der Kolk, J. W. H., Hengeveld, G. M., Lesschen, J. P., Kramer, H., Kuikman, P. J.,  
828 and Schelhaas, M. J.: Greenhouse gas reporting for the LULUCF sector in the Netherlands -  
829 Methodological background, updata 2018, Wageningen, WOt-technical report 113., 2018.
- 830 Asadzadeh, M. and Tolson, B.: Pareto archived dynamically dimensioned search with hypervolume-  
831 based selection for multi-objective optimization, *Eng. Optim.*, 45, 1489–1509,  
832 <https://doi.org/https://doi.org/10.1080/0305215X.2012.748046>, 2013.
- 833 Bechtold, M., Tiemeyer, B., Laggner, A., Leppelt, T., Frahm, E., and Belting, S.: Large-scale  
834 regionalization of water table depth in peatlands optimized for greenhouse gas emission upscaling,  
835 *Hydrol. Earth Syst. Sci.*, 18, 3319–3339, <https://doi.org/10.5194/hess-18-3319-2014>, 2014.
- 836 Bechtold, M., Lannoy, G. J. M. De, Koster, R. D., Reichle, R. H., Mahanama, S. P., Bleuten, W.,  
837 Bourgault, M. A., Brümmer, C., Burdun, I., Desai, A. R., Devito, K., Grünwald, T., Grygoruk, M.,  
838 Humphreys, E. R., Klatt, J., Kurbatova, J., Lohila, A., Munir, T. M., Nilsson, M. B., Price, J. S., Röhl, M.,  
839 Schneider, A., and Tiemeyer, B.: PEAT-CLSM: A Specific Treatment of Peatland Hydrology in the NASA  
840 Catchment Land Surface Model, *J. Adv. Model. Earth Syst.*, 2130–2162,  
841 <https://doi.org/10.1029/2018MS001574>, 2019.
- 842 Børgesen, C. D., Waagepetersen, J., Iversen, T. M., Grant, R., Jacobsen, B., and Elmholt, S.:  
843 Midtvejsevaluering af vandmiljøplan III - Hoved- og baggrundsnotater, 2009.
- 844 DHI: MIKE HYDRO - River - User Guide, Hørsholm, Denmark, 2019.
- 845 DHI: MIKE SHE - User Guide and Reference Manual, Hørsholm, Denmark, 2022.
- 846 Duranel, A., Thompson, J. R., Burningham, H., Durepaire, P., Garambois, S., Wyns, R., and Cubizolle, H.:  
847 Modelling the hydrological interactions between a fissured granite aquifer and a valley mire in the  
848 Massif Central, France, *Hydrol. Earth Syst. Sci.*, 25, 291–319, 2021.
- 849 Evans, C. D., Peacock, M., Baird, A. J., Artz, R. R. E., Burden, A., Callaghan, N., Chapman, P. J., Cooper,  
850 H. M., Coyle, M., Craig, E., Cumming, A., Dixon, S., Gauci, V., Grayson, R. P., Helfter, C., Heppell, C. M.,  
851 Holden, J., Jones, D. L., Kaduk, J., Levy, P., Matthews, R., McNamara, N. P., Misselbrook, T., Oakley, S.,  
852 Page, S. E., Rayment, M., Ridley, L. M., Stanley, K. M., Williamson, J. L., Worrall, F., and Morrison, R.:  
853 Overriding water table control on managed peatland greenhouse gas emissions, *Nature*, 593, 548–552,  
854 <https://doi.org/10.1038/s41586-021-03523-1>, 2021.
- 855 Friedrich, S., Gerner, A., Gabrielle, C., and Disse, M.: Scenario-based groundwater modeling of a raised  
856 bog with Mike She, EGU Gen. Assem. 2023, Vienna, Austria, 24–28 Apr 2023, EGU23-15608,  
857 <https://doi.org/https://doi.org/10.5194/egusphere-egu23-15608>, 2023.
- 858 Jupiter: [https://www.geus.dk/produkter-ydelser-og-faciliteter/data-og-kort/national-boringsdatabase-](https://www.geus.dk/produkter-ydelser-og-faciliteter/data-og-kort/national-boringsdatabase-jupiter)  
859 [jupiter](https://www.geus.dk/produkter-ydelser-og-faciliteter/data-og-kort/national-boringsdatabase-jupiter), last access: 12 April 2025.
- 860 Graham, D. N. and Butts, M. B.: Flexible Integrated Watershed Modeling with MIKE SHE, in: *Watershed*  
861 *Models*, edited by: Singh, V. P. and Frevert, D. K., CRC Press, 245–272,  
862 <https://doi.org/10.1201/9781420037432.ch10>, 2005.
- 863 Günther, A., Barthelmes, A., Huth, V., Joosten, H., Jurasinski, G., Koebisch, F., and Couwenberg, J.:  
864 Prompt rewetting of drained peatlands reduces climate warming despite methane emissions, *Nat.*  
865 *Commun.*, 11, 1–5, <https://doi.org/10.1038/s41467-020-15499-z>, 2020.
- 866 Gyldenkerne, S., Callisen, L. W., Greve, M. H., Beucher, A. M., Weber, P. L., Elsgaard, L., Lærke, P. E.,  
867 Stisen, S., Koch, J., and Levin, G.: Opgørelse af CO<sub>2</sub>-emissioner fra organiske jorde, Aarhus Universitet,  
868 DCE – Nationalt Center for Miljø og Energi, Fagligt notat nr. 2025|01, 29pp pp., 2025.





- 869 Haahti, K., Warsta, L., Kokkonen, T., Younis, B. B., and Koivusalo, H.: Distributed hydrological modeling  
870 with channel network flow of a forestry drained peatland site, *Water Resour. Res.*, 246–263,  
871 <https://doi.org/10.1002/2015WR018038>. Received, 2015.
- 872 Henriksen, H. J., Kragh, S. J., Gotfredsen, J., Ondracek, M., M, van, T., Jakobsen, A., Schneider, R., Koch,  
873 J., Trolborg, L., Rasmussen, P., Pasten-Zapata, E., and Stisen, S.: Dokumentationsrapport vedr.  
874 modelleverancer til Hydrologisk Informations- og Prognosesystem, 2020.
- 875 Henriksen, H. J., Schneider, R., Koch, J., Ondracek, M., Trolborg, L., Seidenfaden, I. K., Kragh, S. J.,  
876 Bøgh, E., and Stisen, S.: A New Digital Twin for Climate Change Adaptation, Water Management, and  
877 Disaster Risk Reduction (HIP Digital Twin), *Water (Switzerland)*, 15,  
878 <https://doi.org/10.3390/w15010025>, 2023.
- 879 IPCC: 2013 Supplement to the 2006 IPCC Guidelines for National Greenhouse Gas Inventories :  
880 Wetlands, edited by: Hiraishi, T., Krug, T., Tanabe, K., Srivastava, N., Baasansuren, J., Fukuda,  
881 M. Troxler, T. G., Published: IPCC, Switzerland, Switzerland, 2014.
- 882 Jacob, D., Petersen, J., Eggert, B., Alias, A., Christensen, O. B., Bouwer, L. M., Braun, A., Colette, A.,  
883 Déqué, M., Georgievski, G., Georgopoulou, E., Gobiet, A., Menut, L., Nikulin, G., Haensler, A.,  
884 Hempelmann, N., Jones, C., Keuler, K., Kovats, S., Kröner, N., Kotlarski, S., Kriegsmann, A., Martin, E.,  
885 van Meijgaard, E., Moseley, C., Pfeifer, S., Preuschmann, S., Radermacher, C., Radtke, K., Rechid, D.,  
886 Rounsevell, M., Samuelsson, P., Somot, S., Soussana, J. F., Teichmann, C., Valentini, R., Vautard, R.,  
887 Weber, B., and Yiou, P.: EURO-CORDEX: New high-resolution climate change projections for European  
888 impact research, *Reg. Environ. Chang.*, 14, 563–578, <https://doi.org/10.1007/s10113-013-0499-2>,  
889 2014.
- 890 Java, O., Kohv, M., and Löhmus, A.: Performance of a bog hydrological system dynamics simulation  
891 model in an ecological restoration context: Soomaa case study, Estonia, *Water (Switzerland)*, 13,  
892 <https://doi.org/10.3390/w13162217>, 2021.
- 893 Jutebring, E., Johansson, E., Sjöberg, Y., Huseby, R., and Laudon, H.: Groundwater-surface water  
894 interactions across scales in a boreal landscape investigated using a numerical modelling approach, *J.*  
895 *Hydrol.*, 560, 184–201, <https://doi.org/10.1016/j.jhydrol.2018.03.011>, 2018.
- 896 Kirpotin, S. N., Antoshkina, O. A., Berezin, A. E., Elshehawi, S., Feurdean, A., Lapshina, E. D., Pokrovsky,  
897 O. S., Peregon, A. M., Semenova, N. M., Tanneberger, F., Volkov, I. V., and Volkova, I. I.: Great Vasyugan  
898 Mire: How the world ' s largest peatland helps addressing the world ' s largest problems, *Ambio*, 50,  
899 2038–2049, <https://doi.org/10.1007/s13280-021-01520-2>, 2021.
- 900 Koch, J., Elsgaard, L., Greve, M. H., Gyldenkerne, S., Hermansen, C., Levin, G., Wu, S., and Stisen, S.:  
901 Water-table-driven greenhouse gas emission estimates guide peatland restoration at national scale,  
902 *Biogeosciences*, 20, 2387–2403, <https://doi.org/https://doi.org/10.5194/bg-20-2387-2023>, 2023.
- 903 Langeron, C., Krinner, G., Ciais, P., and Brutel-Vuilmet, C.: Implementing northern peatlands in a global  
904 land surface model: Description and evaluation in the ORCHIDEE high-latitude version model (ORC-HL-  
905 PEAT), *Geosci. Model Dev.*, 11, 3279–3297, <https://doi.org/10.5194/gmd-11-3279-2018>, 2018.
- 906 Leifeld, J., Wüst-Galley, C., and Page, S.: Intact and managed peatland soils as a source and sink of  
907 GHGs from 1850 to 2100, *Nat. Clim. Chang.*, 9, 945–947, <https://doi.org/10.1038/s41558-019-0615-5>,  
908 2019.
- 909 Lewis, C., Albertson, J., Zi, T., Xu, X., and Kiely, G.: How does afforestation affect the hydrology of a  
910 blanket peatland? A modelling study, *Hydrol. Process.*, 3588, 3577–3588,  
911 <https://doi.org/10.1002/hyp.9486>, 2013.
- 912 Lloyd J., Taylor, J. A.: On the Temperature Dependence of Soil Respiration, *Funct. Ecol.*, 8, 315–323,  
913 1994.



- 914 Matott, L. S.: OSTRICH – An Optimization Software Toolkit for Research Involving Computational  
915 Heuristics Documentation and User ' s Guide, Version 17.12.19, New York, 2019.
- 916 Mozafari, B., Bruen, M., Donohue, S., Renou-wilson, F., and Loughlin, F. O.: Peatland dynamics: A  
917 review of process-based models and approaches Science of the Total Environment Peatland dynamics :  
918 A review of process-based models and approaches, *Sci. Total Environ.*, 877,  
919 <https://doi.org/10.1016/j.scitotenv.2023.162890>, 2023.
- 920 Nielsen, A. S., Larsen, K. S., Lærke, P. L., Rodriguez, A. F., Pullens, J. W. M., Petersen, R. J., and  
921 Christiansen, J. R.: A full year of continuous net soil and ditch CO<sub>2</sub>, CH<sub>4</sub>, N<sub>2</sub>O fluxes, soil hydrology and  
922 meteorology for a drained fen in Denmark, *Earth Syst. Sci. Data Discuss.* [preprint],  
923 <https://doi.org/10.5194/essd-2025-123>, in review, 2025a.
- 924 Nielsen, O.-K., Plejdrup, M. S., Winther, M., Nielsen, M., Gyldenkerne, S., Mikkelsen, M. H.,  
925 Albrektsen, R., Hjelgaard, K., Fauser, P., Bruun, H. G., Levin, G., Callisen, L. W., Andersen, T. A.,  
926 Johannsen, V. K., Nord-Larsen, T., Vesterdal, L., Stupak, I., Scott-Bentsen, N., Rasmussen, E., Petersen,  
927 S. B., Baunbæk, L., and Hansen, M. G.: Denmark's National Inventory Document 2025. Emission  
928 Inventories 1990-2023 - Submitted under the United Nations Framework Convention on Climate  
929 Change and the Paris Agreement, 2025b.
- 930 Olefeldt, D., Euskirchen, E. S., Harden, J., Kane, E., McGuire, A. D., Waldrop, mark P., and Turetsky, M.  
931 R.: A decade of boreal rich fen greenhouse gas fluxes in response to natural and experimental water  
932 table variability, *Glob. Chang. Biol.*, 23, 2428–2440, <https://doi.org/10.1111/gcb.13612>, 2017.
- 933 Pasten-Zapata, E., Sonnenborg, T. O., and Refsgaard, J. C.: Climate change: Sources of uncertainty in  
934 precipitation and temperature projections for Denmark, *Geol. Surv. Denmark Greenl. Bull.*, 43, 1–6,  
935 <https://doi.org/10.34194/GEUSB-201943-01-02>, 2019.
- 936 Regeringen: Aftale om et Grønt Danmark - Aftale mellem regeringen, Landbrug & Fødevarer,  
937 Danmarks Naturfredningsforening, Fødevarerforbundet NNF, Dansk Metal, Dansk Industri og  
938 Kommunernes Landsforening - 24. juni 2024, 2024.
- 939 Regulation (EU) 2024/1991: of the European Parliament and of the Council of 24 June 2024 on nature  
940 restoration and amending Regulation (EU) 2022/869, *Official Journal of the European Union*, 2024.
- 941 Rigney, C., Wilson, D., Renou-Wilson, F., Müller, C., Moser, G., and Byrne, K. A.: Greenhouse gas  
942 emissions from two rewetted peatlands previously managed for forestry, *Mires Peat*, 21, 1–23,  
943 <https://doi.org/10.19189/MaP.2017.OMB.314>, 2018.
- 944 Rodriguez, A. F., Pullens, J. W. M., Christiansen, J. R., Larsen, K. S., and Lærke, P. E.: Modeling of  
945 greenhouse gas emissions from paludiculture in rewetting peatlands is improved by high frequency  
946 water table data, *Egusph.* [preprint], <https://doi.org/10.5194/egusphere-2024-3030>, 2024.
- 947 Scharling, M.: Klimagrid Danmark - Nedbør, lufttemperatur og potentiel fordampning 20X20 & 40x40  
948 km - Metodebeskrivelse, Danish Meteorological Institute, 1999a.
- 949 Scharling, M.: Klimagrid Danmark Nedbør 10x10 km (ver. 2) - Metodebeskrivelse, Danish  
950 Meteorological Institute, 1999b.
- 951 Schneider, R., Koch, J., Trolborg, L., Henriksen, H. J., and Stisen, S.: Machine learning-based  
952 downscaling of modelled climate change impacts on groundwater table depth, 2022.
- 953 Seidenfaden, I. K., Sonnenborg, T. O., Stisen, S., and Kidmose, J.: Quantification of climate change  
954 sensitivity of shallow and deep groundwater in Denmark, *J. Hydrol. Reg. Stud.*, 41, 101100,  
955 <https://doi.org/10.1016/j.ejrh.2022.101100>, 2022.
- 956 Shi, X., Thornton, P. E., Ricciuto, D. M., Hanson, P. J., Mao, J., Sebestyen, S. D., Griffiths, N. A., and  
957 Bisht, G.: Representing northern peatland microtopography and hydrology within the Community Land



- 958 Model, Biogeosciences, 12, 6463–6477, <https://doi.org/10.5194/bg-12-6463-2015>, 2015.
- 959 Stenberg, L., Haahti, K., Hökkä, H., Launiainen, S., and Nieminen, M.: Hydrology of Drained Peatland  
960 Forest: Numerical Experiment on the Role of Tree Stand Heterogeneity and Management, For. MDPI,  
961 1–19, <https://doi.org/10.3390/f9100645>, 2018.
- 962 Stisen, S., Sonnenborg, T. O., Trolborg, L., and Refsgaard, J. C.: Evaluation of Climate Input Biases and  
963 Water Balance Issues Using a Coupled Surface – Subsurface Model, Vadose Zo. J., 10,  
964 <https://doi.org/10.2136/vzj2010.0001>, 2011.
- 965 Stisen, S., Ondracek, M., Trolborg, L., Schneider, R. J. M., and van Til, M. J.: National Vandressource  
966 Model - Modelopstilling og kalibrering af DK-model 2019, De nationale geologiske undersøgelser for  
967 Danmark og Grønland (GEUS), Rapport 2019/31, 2019.
- 968 Tanneberger, F., Abel, S., Couwenberg, J., Dahms, T., Gaudig, G., Günther, A., Kreyling, J., Peters, J.,  
969 Pongratz, J., and Joosten, H.: Towards net zero CO<sub>2</sub> in 2050: An emission reduction pathway for  
970 organic soils in germany, Mires Peat, 27, 1–17, <https://doi.org/10.19189/MaP.2020.SNPG.StA.1951>,  
971 2021.
- 972 Tiemeyer, B., Freibauer, A., Borraz, E. A., Augustin, J., Bechtold, M., Beetz, S., Beyer, C., Ebli, M.,  
973 Eickenscheidt, T., Fiedler, S., Förster, C., Gensior, A., Giebels, M., Glatzel, S., Heinichen, J., Hoffmann,  
974 M., Höper, H., Jurasinski, G., Laggner, A., Leiber-Sauheitl, K., Peichl-Brak, M., and Drösler, M.: A new  
975 methodology for organic soils in national greenhouse gas inventories: Data synthesis, derivation and  
976 application, Ecol. Indic., 109, 105838, <https://doi.org/10.1016/j.ecolind.2019.105838>, 2020.
- 977 Wilson, D., Blain, D., Couwenber, J., Evans, C., Murdiyarso, D., Page, S., Renou-Wilson, F., Rieley, J.,  
978 Strack, M., and Tuittila, E. S.: Greenhouse gas emission factors associated with rewetting of organic  
979 soils, Mires Peat, 17, 1–28, <https://doi.org/10.19189/MaP.2016.OMB.222>, 2016.
- 980 Wunsch, A., Liesch, T., and Broda, S.: Deep learning shows declining groundwater levels in Germany  
981 until 2100 due to climate change, Nat. Commun., 13, 1–13, [https://doi.org/10.1038/s41467-022-](https://doi.org/10.1038/s41467-022-28770-2)  
982 28770-2, 2022.
- 983 Yuan, F., Wang, Y., Ricciuto, D. M., Shi, X., Yuan, F., Brehme, T., Bridgham, S., Keller, J., Warren, J. M.,  
984 Griffiths, N. A., Sebestyen, S. D., Hanson, P. J., Thornton, P. E., and Xu, X.: Hydrological feedbacks on  
985 peatland CH<sub>4</sub> emission under warming and elevated CO<sub>2</sub>: A modeling study, J. Hydrol., 603, 127137,  
986 <https://doi.org/10.1016/j.jhydrol.2021.127137>, 2021.
- 987 Zscheischler, J., Martius, O., Westra, S., Bevacqua, E., Raymond, C., Horton, R. M., van den Hurk, B.,  
988 AghaKouchak, A., Jézéquel, A., Mahecha, M. D., Maraun, D., Ramos, A. M., Ridder, N. N., Thiery, W.,  
989 and Vignotto, E.: A typology of compound weather and climate events, Nat. Rev. Earth Environ., 1,  
990 333–347, <https://doi.org/10.1038/s43017-020-0060-z>, 2020.

991

992